CHARM HADRON PRODUCTION IN HIGH ENERGY ELECTRON-PROTON COLLISIONS

NUR ZULAIHA JOMHARI

FACULTY OF SCIENCE
UNIVERSITY OF MALAYA
KUALA LUMPUR

2017

CHARM HADRON PRODUCTION IN HIGH ENERGY ELECTRON-PROTON COLLISIONS

NUR ZULAIHA JOMHARI

DISSERTATION SUBMITTED IN FULFILMENT OF THE REQUIREMENTS FOR THE DEGREE OF MASTER OF SCIENCE (EXCEPT MATHEMATICS & SCIENCE PHILOSOPHY)

DEPARTMENT OF PHYSICS
FACULTY OF SCIENCE
UNIVERSITY OF MALAYA
KUALA LUMPUR

2017

UNIVERSITI MALAYA

ORIGINAL LITERARY WORK DECLARATION

Name of Candidate: **Nur Zulaiha Jomhari**

Registration/Matrix No.: **SGR130089**

Name of Degree: **Master of Science (Except Mathematics and Philosophy)**

Title of Project Paper/Research Report/Dissertation/Thesis ("this Work"):

Charm Hadron Production in High Energy Electron-Proton Collisions

Field of Study: **Experimental Physics**

    I do solemnly and sincerely declare that:

(1) I am the sole author/writer of this Work;
(2) This work is original;
(3) Any use of any work in which copyright exists was done by way of fair dealing and for permitted purposes and any excerpt or extract from, or reference to or reproduction of any copyright work has been disclosed expressly and sufficiently and the title of the Work and its authorship have been acknowledged in this Work;
(4) I do not have any actual knowledge nor do I ought reasonably to know that the making of this work constitutes an infringement of any copyright work;
(5) I hereby assign all and every rights in the copyright to this Work to the University of Malaya ("UM"), who henceforth shall be owner of the copyright in this Work and that any reproduction or use in any form or by any means whatsoever is prohibited without the written consent of UM having been first had and obtained;
(6) I am fully aware that if in the course of making this Work I have infringed any copyright whether intentionally or otherwise, I may be subject to legal action or any other action as may be determined by UM.

    Candidate's Signature   Date

Subscribed and solemnly declared before,

    Witness's Signature   Date

Name:
Designation:

ABSTRACT

Exclusive events are the events that focus on one specific physics signature such as selecting events that contained only three tracks and nothing else. D meson is the lightest meson containing charm quarks and interact via weak interaction which make it easier to study its decay product. In this thesis, both inclusive and exclusive searches of $D^{\pm}$ meson decaying to $K^{-}\pi^{+}\pi^{+}$ in deep inelastic electron-proton scattering are presented. It is interesting to do this search as exclusive $D^{\pm}$ is not expected to be observed, which has to be experimentally verified. The search was done using data collected by the ZEUS experiment, one of the 4 major experiments of the HERA-II collider. The data used was taken from 2003 - 2007 at a center of the mass energy 318 GeV. Two Monte Carlo (MC) samples are used and combined to compare with data; non-diffractive and diffractive MC. The relative fractions in non-diffractive and diffractive mixture are calculated and compared in order to select which fraction suit the best that describes the events in data.

ABSTRAK

Didalam fizik zarah, kejadian eksklusif merupakan kejadian yang hanya fokus pada spesifik ciri fizik yang tersendiri seperti memilih kejadian yang hanya mempunyai 3 trek sahaja. D meson merupakan meson yang paling ringan mengandungi *charm* kuark dan berinteraksi melalui interaksi lemah membuatkan pereputan daripada D meson dapat difahami dan dikaji dengan lebih mudah. Di dalam tesis ini, kedua-dua pencarian inklusif dan eksklusif $D^{\pm}$ yang mereput kepada $K^- \, pi^+ \, pi^+$ dalam pelanggaran tidak kenyal dibentangkan. Penyelidikan ini menarik untuk dilakukan kerana eksklusif $D^{\pm}$ tidak dijangka dapat dilihat melalui experiment. Pencarian ini dilakukan dengan menggunakan data yang dikumpul oleh eksperimen ZEUS; salah satu 4 eksperimen utama di pelanggar HERA-II. Data yang digunakan diambil dari tahun 2003-2007 pada tenaga pusat 318 GeV. Dua sampel Monte Carlo (MC) diguna dan digabungkan untuk dibandingkan dengan data iaitu *non-diffractive* MC dan *diffractive* MC. Pecahan relatif dan campuran kedua-dua MC dikira dan dibandingkan untuk memilih pecahan yang paling sesuai menggambarkan kejadian yang berlaku di dalam data.

ACKNOWLEDGEMENTS

I would like to express my gratitude to several people who are patiently helping my journey throughout producing this thesis.

First of all is my supervisor, Prof. Wan Ahmad Tajuddin Wan Abdullah for gave me the opportunity to enter particle physic's world which I don't know about because of my ignorant. Thank you for your suggestions and ideas that help me improved my thesis. Other than that is Prof. Zainol Abidin Ibrahim, thank you for your advices in life and sharing your experience.

I am also indebted to my ZEUS collaborators especially Achim Geiser for your trust, guidance and the most important, the opportunity you gave me. Not forget to Anya, Jenya, Misha, Matthew, Oleg, Janusz and others who spent their time to teach a newbie like me and guided me during my first stay at DESY and even remotely through emails. I really appreciate your help.

Moreover, special thanks to my colleagues and friends whom I interact the most during my three years of doing master degree. That people are Atikah; my ZEUS partner, Kak Najwa and Syazana; my roommates and Afiq; my bestfriend. We laugh together, share opinion, argued a lot but we help each other physically and emotionally.

Not forget to my family, mainly my mom (ma) and dad (abah) for your love and kindness endlessly.

To my late dad (pa), I miss you.

I was lucky to have wonderful people around me. Thank you so much.

TABLE OF CONTENT

LIST OF FIGURES

LIST OF TABLES

LIST OF SYMBOLS AND ABBREVIATIONS

BCAL   :   Barrel Calorimeter
BGF   :   Boson-Gluon Fusion
BMVD :   Barrel Micro Vertex Detector
BNL   :   Brookhaven National Laboratory
CAL   :   Uranium Scintillator Calorimeter
CC   :   Charge Current
CTD   :   Central Tracking Detector
DA   :   Double Angle
DAS   :   Deterministic Annealing Filter
DCA   :   Distance Closest Approach
DIS   :   Deep Inelastic electron-proton Scattering
e-p   :   electron-proton
EFOs   :   Energy Flow Objects
EM   :   Electromagnetic
EMC   :   Electromagnetic Calorimeter
FCAL   :   Forward Calorimeter
FLT   :   First Level Trigger
FMVD :   Forward Micro Vertex Detector
HAC   :   Hadronic Calorimeter
HERA :   Hadron Elektron Ring Anlage
JB   :   Jaquet-Blondel
MC   :   Monte Carlo
MVD   :   Micro Vertex Detector
PHP   :   Photoproduction
pQCD   :   perturbative Quantum Chromodynamics
QCD   :   Quantum Chromodynamics
QED   :   Quantum Electrodynamics
QPM   :   Quark Parton Model
RCAL   :   Rear Calorimeter
SLAC   :   Stanford Linear Accelerator Center
SLT   :   Second Level Trigger
SM   :   Standard Model
STT   :   Straw Tube Tracker
TLT   :   Third Level Trigger
VXD   :   Vertex Detector
ZEVis   :   ZEUS Visualization
ZUFOs :   ZEUS Unidentified Flow Objects

CHAPTER 1: INTRODUCTION

The interactions between fundamental particles are mediated by the force carriers and are described in the Standard Model (SM) (Weinberg, 1967; Glashow et al., 1970a). In SM, there are two types of particles. First are the spin $-\frac{1}{2}$ particles called fermions, which are divided into quarks and leptons. Secondly, there are the spin -1 particles called gauge bosons. There is also the Higgs boson, which is a spin -0 particle that became the major discovery in Particle Physics field because it solved the issue of massive $W^{\pm}$ and Z bosons and confirmed the accuracy of SM. An overview of Standard Model is shown in Figure 1.1[1].

Quarks come in 6 flavours; up, down, charm, strange, top and bottom and they are categorized in 3 generations. They have fractional electric charge; the up-type quarks have $+\frac{2}{3}$ charge[2] while the down-type quarks have $-\frac{1}{3}$ charge. However, quark itself is not observable as a free particle, instead, combination of quarks does. Meson is composed of one quark and one anti-quark while baryon is combination of three quarks. Both fall into a family of hadron; composite particle of quarks held together by gluon in strong interaction.

Similarly, leptons come in 6 flavours, electron neutrino, electron, muon neutrino, muon, tau neutrino and tau. Neutrinos are electrically neutral while the rest have -1 charge. The charged leptons interact via electromagnetic and weak interactions while neutrinos only through the weak interaction.

So far, only one force that does not include in SM which is gravity. Since gravitational interaction between fundamental particles is very small and graviton is still not

---

[1]Picture taken from particle fever:http://particlefever.com/ (5 Nov. 2016)

[2]Charge is always a multiple of e whenever relevant in this thesis
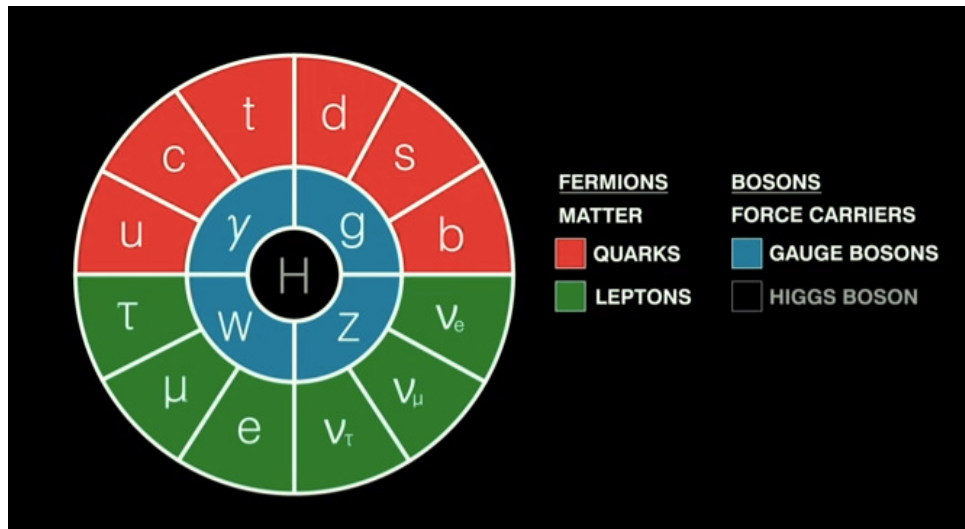
Figure 1.1: List of the particles in SM.

yet observed in the experiments, this interaction can be neglected at presently accessible

energies. Each force have their own mediator. For example, mediator for strong force is

called gluon, for electromagnetic force is photon, for weak force is $W^{\pm}$ and Z. Each of

these mediators have different characteristics as shown in Figure 1.2[3].

Particle accelerator provides high energies to particles for collision while particle

detectors observe the interaction of these particles. This analysis is conducted in ZEUS

experiment. In the ZEUS experiment, the particle accelerator is called HERA and the

detector is called ZEUS detector. HERA accelerator is the first accelerator that study the

electron-proton (e-p) collision and ZEUS detector is used to detect, keep track and collect

the data of new particles produced from this collision. More details will be discussed in

Chapter 3.

Among the interesting interactions to be studied is the production of charm mesons.

Charm mesons are mesons that contain one charm quark[4] in the quark pair. Since charm

---

[3]Picture taken from NOVA website:

http://www.pbs.org/wgbh/nova/education/activities/3012_elegant_02.html (5 Nov. 2016)

[4]Charge conjugation is implied here and throughout the thesis whenever relevant

Force	Particles Experiencing	Force Carrier Particle	Range	Relative Strength*
Gravity acts between objects with mass	all particles with mass	graviton (not yet observed)	infinity	much weaker
Weak Force governs particle decay	quarks and leptons	W^+, W^-, Z^0 (W and Z)	short range	
Electromagnetism acts between electrically charged particles	electrically charged	γ (photon)	infinity	
Strong Force** binds quarks together	quarks and gluons	g (gluon)	short range	much stronger

Figure 1.2: List of interactions and their mediators in SM.

quark is considered as heavy quark as the mass is high ($m_c \gg \lambda_{QCD}$), perturbative Quantum Chromodynamics (pQCD) approach can be used.

This thesis is focused on the search for exclusive charm meson which is $D^\pm$ in deep inelastic scattering process where only an electron and a $D^\pm$ is found in the events. D^+ consist of one charm quark and one anti-down quark and it decay to $K^-\pi^+\pi^+$ that has $\bar{u}s$, $u\bar{d}$ and $u\bar{d}$ quark respectively.

1.1 Objectives

The objectives of this research are:

1. To reproduce the mass of inclusive $D^\pm$ of HERA II in Deep Inelastic electron-proton Scattering (DIS) process of electron-proton collisions.

2. To search for exclusive $D^\pm$ in HERA II dataset.

1.2 Thesis Outline

This thesis is arranged into several chapters as follows. This chapter give an introduction about the basics of particle physics in general, problem statement, the motivation of the thesis and the thesis outline. Chapter 2 describes the physics and kinematics involved in the search for charm particle during electron-proton collisions. Chapter 3 describes the experimental setup of HERA accelerator and the ZEUS detector components that are relevant to this research. Next, the details of the event reconstruction is elaborated in Chapter 4. The selection of the event and $D^{\pm}$ reconstruction used for this analysis is continued in Chapter 5. Chapter 6 shows the results of inclusive $D^{\pm}$ compared with the previous paper and also the implementation of exclusive cuts and qualitative measurement of quasi-exclusive $D^{\pm}$ is presented. Lastly, Chapter 7 concludes the entire work.

CHAPTER 2: ELECTRON-PROTON COLLISIONS

2.1 Introduction

This chapter will describe the physics involved in this research at HERA. At the beginning two classes of electron-proton scattering and the event kinematics is given. Then the theoretical model is briefly explained and lastly the chapter ends with the charm production mechanism.

2.2 Deep Inelastic Electron-Proton Scattering at HERA

DIS is the process where an incoming electron collides with a constituent parton inside the proton and knocks out the quark of the proton. As a result, the proton broke up and multiple hadronic particles are produced denoted as X in Figure 2.1. Another type of process is Photoproduction (PHP) process which is photon-proton interaction. In DIS, the virtuality of the exchanged boson, Q^2 is higher compared to PHP where the Q^2 is close to zero. The comparison of these processes at HERA is explained in (Aid et al., 1995).

The interaction of electron and proton is described by the exchange of a vector boson. For Charge Current (CC) process, the exchanged boson involved is $W^{\pm}$ with a neutrino as a final state particle while for the NC process, it can be photon (γ) or Z^0 leaves scattered electron in the final state. In this thesis, NC process is selected as it has higher cross-section compared to CC process.

The interaction of NC and CC processes is labelled in Equation 2.1 and 2.2 respectively.

$$e^{\pm} + p \rightarrow e^{\pm} + X \tag{2.1}$$

$$e^+(e^-) + p \rightarrow \nu_e(\bar{\nu}_e) + X \tag{2.2}$$
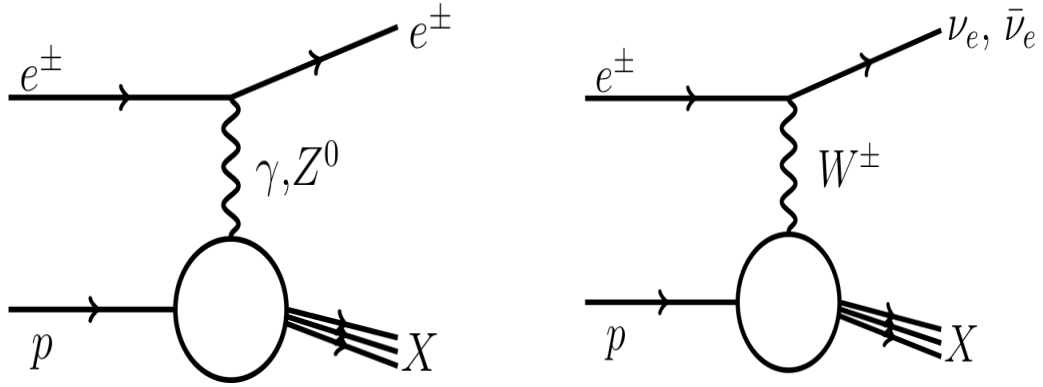
Figure 2.1: Lowest order Feynman diagrams for Neutral Current (left) and Charge Current (right) process in DIS.
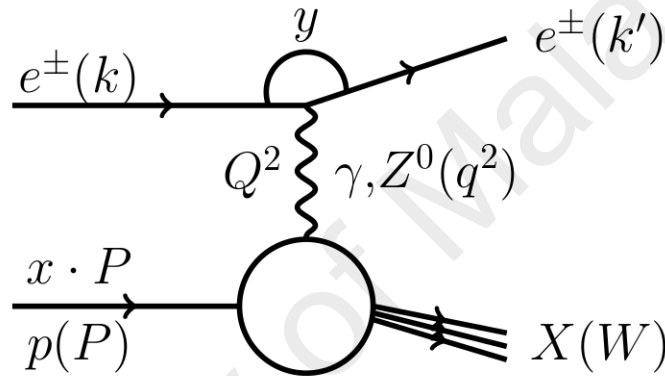
Figure 2.2: Kinematic variables involve in electron-proton scattering.

2.2.1 Kinematics

Figure 2.2 shows Feynman diagram of NC electron-proton scattering and the kinematic variables at HERA. Let k, k' and P be the initial 4-momentum of electron, final 4-momentum of electron and initial 4-momentum of proton respectively. Then the momentum transfer q between electron and proton is given by

$$q = k' - k \tag{2.3}$$

The scattering process is characterized by the following Lorentz invariant variables (Abramowicz & Caldwell, 1999):

- The center-of-mass energy squared in the elecron-proton system, s

$$s = (k + P)^2 \approx 2k \cdot p = \frac{Q^2}{xy} \tag{2.4}$$

- Negative square of the momentum transfer, the so-called exchanged boson virtuality, Q^2

$$Q^2 = -q^2 = -(k - k')^2 \tag{2.5}$$

where events of $Q^2 \gg 1\text{GeV}^2$ are DIS events.

- Bjorken scaling variable (Bjorken & Paschos, 1969), x

$$x = \frac{Q^2}{2P \cdot q} \tag{2.6}$$

In proton infinite momentum frame, it can be interpreted as the fraction of proton's momentum carried by the parton (quark or gluon). At HERA the laboratory frame behaves like infinite momentum frame.

- Fraction of the electron energy transferred to hadronic system in proton rest frame, also called inelasticity, y

$$y = \frac{P \cdot q}{P \cdot k} \tag{2.7}$$

- Center-of-mass energy squared of the final hadronic system, W^2

$$W^2 = (P + q)^2 \simeq sy - Q^2 \tag{2.8}$$

Kinematic variables x, y and s are not independent if the masses of the electron and proton are neglected. They are correlated to each other by (Whyte, 2008):

$$Q^2 = s \cdot x \cdot y \qquad (2.9)$$

At HERA II, the center-of-mass energy was fixed to 318 GeV, left only x and y as an independent variables. Therefore, the inclusive DIS scattering kinematics can be decribed by the combination of any of these two variables, x, Q^2 or y, Q^2.

2.3 Quark Parton Model

The parton model described that proton is built up of point-like constituents called partons. The model also helped interpret the structure of the proton and neutron in DIS experiment. This model was introduced by Feynman which suggested simple calculation of scattering cross section to explain a feature observed in DIS data of Stanford Linear Accelerator Center (SLAC) (Feynman, 1969) while Bjorken proved the scattering of high-energy electrons on the proton were independent of Q^2 named *scaling* (Bjorken, 1969). One way to validate this model is by comparing the way of the cross-section behaves since it depends on the proton structure function.
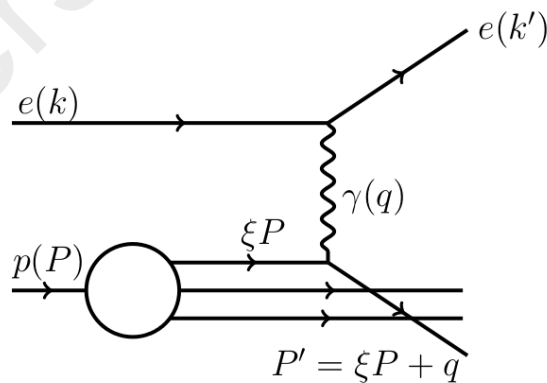
Figure 2.3: Schematic of parton-photon interaction.

Figure 2.3 shows that the photon momentum, q interacts with the parton inside the proton and carries a fraction, ξ of proton momentum, P. The momentum of the outgoing

parton is given by $P' = \xi P + q$.

Neglecting the parton and proton masses and using conservation of momentum we obtain:

$$P'^2 = (\xi P + q)^2 = \xi^2 P^2 + 2\xi Pq + q^2 \approx 2\xi Pq - Q^2 \approx 0 \qquad (2.10)$$

Rearrange equation above will give fraction of proton momentum:

$$\xi = \frac{Q^2}{2P \cdot q} = x \qquad (2.11)$$

From Equation 2.11, it can be concluded that Bjorken scaling variable, x can be defined as the fraction of proton momentum carried by parton in scattering process.

Bjorken predicted in the late sixties that structure functions of proton, $F_{1,2}$ can be interpreted as the sum of parton densities:

$$F_2(x, Q^2) = F_2(x) = \sum_i e_i^2 x f_i(x), \qquad (2.12)$$

$$F_1(x, Q^2) = F_1(x) = \frac{1}{2x} F_2(x) \qquad (2.13)$$

where e_i is the the charge of parton i and $f_i(x)$ is the parton distribution function. This Equation 2.12 is known as Callan-Gross relation (Callan & Gross, 1969). The parton model led to identification of partons as the quarks called Quark Parton Model (QPM). More specific details including all the calculations can be found in (Greenberg, 2008).

However, from the experimental observation, quarks are not the only constituent of proton because the sum of quarks momenta are not equal to the sum of proton momentum. It is found that the fraction of proton momentum carried by the quarks is approximately 0.5, which means the other half of the momentum is from other particles and the reason will be described in the next topic, Quantum Chromodynamics.

2.4 Quantum Chromodynamic

Quantum Chromodynamics (QCD) is an improved model from QPM and it is a theory that explained the strong interaction of quarks and gluons to form hadrons. The evidence of gluon existence was confirmed in electron-positron collision at DESY that observed 3 jets events (Brandelik et al., 1979). QCD introduced the word "colour" from the prefix chromo which described the property of quarks and gluons in strong interaction called "colour-charge". A particle can have either red, blue or green charge while antiparticle can be anti-red, anti-blue or anti-green to conserve the charge. Combination of these three quarks (baryon) or any one of these colours with their anti-colour (meson) will produced colourless charge or zero colour charge.

In QCD, the strong force carried by gluon gets stronger when the quarks are pulled apart and it is contrast with the Quantum Electrodynamics (QED) where the Electromagnetic (EM) force carried by photon gets weaker as distance of particles increases. This is because at high separation between the two quarks, it have enough energy to create the new quark and anti-quark pairs leading to new bound states called hadrons in a process called hadronisation. As a result, quarks and gluons cannot be observed as a free particles yet experimentalist observed group of colourless hadrons in cone shapes named jets.

The strength of parton interaction is determined by strong coupling constant, α_s and it varies with Q^2. The higher the Q^2, the smaller the distance resolved inside the proton and the smaller the value of α_s. The value of α_s at leading order is given as:

$$\alpha_s(\mu_R^2) = \frac{12\pi}{33 - 2n_f ln(\frac{\mu_R^2}{\Lambda_{QCD}^2})} \tag{2.14}$$

where (μ_R^2) is the renormalisation scale, n_f is the number of active light quark flavours with mass less than μ and Λ_{QCD} is the QCD cutoff parameter where experimentally the

value is determined to be 200 MeV.

Quarks can emit gluons and the gluons can split into a pair of sea-quarks or interact with themselves. This will result in the increase of partons number but decrease in average momentum of partons. The number of valence quarks, sea quarks and gluons depend on the scale of interaction as shown in Figure 2.4 below.
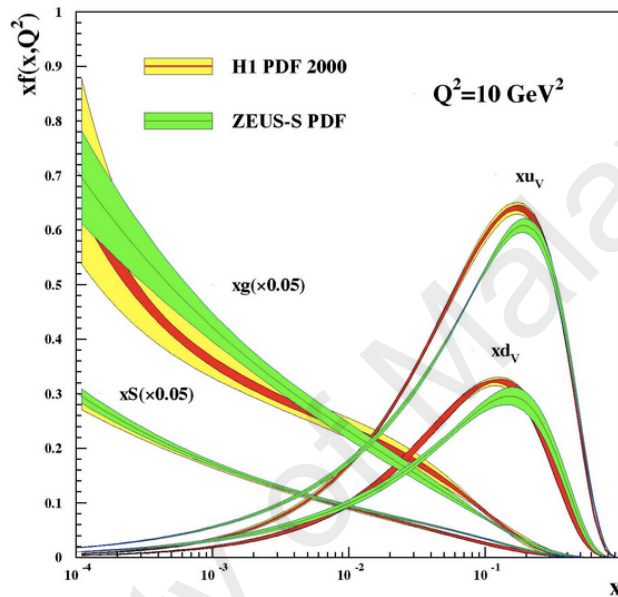
Figure 2.4: Parton distribution function at $Q^2 = 10$ GeV^2 of valence quarks up (u) and down (d), gluon (g) and sea (S) quarks.

Figure 2.4[1] shows that the fractional momentum, x of up valence quarks is twice of the fractional momentum x of down valence quarks. This indicated that proton contained two up valence quarks and one down valence quark. At low values of x, it can be seen that gluons and sea quarks dominate the proton fractional momentum and become smaller at high values of x.

---

[1]Picture taken from website: http://www.mit.edu/~hasell/DKH_zeus.html

2.5 Charm Quark Production

A question arise on how does a charm quark exist in electron-proton collision considering the mass of charm quark is greater than the mass of proton. In 1970s, there were questions regarding the non-observation of several meson decay modes such as $K^0 \rightarrow \mu^+ \mu^-$. Glashow, Iliopoulos and Maiani proposed the GIM mechanism (Glashow et al., 1970b) that explained this observations but required the existence of a forth quark state which is now known as charm quark. It is proven in 1974 where the first charm quarks were observed at SLAC and Brookhaven National Laboratory (BNL). The charm quarks were bound with anti-charm quarks ($c\bar{c}$) and known as J/ψ meson.

At HERA, Boson-Gluon Fusion (BGF) mechanism is the main contribution for the charm quark production (Behnke et al., 2015). Figure 2.5 shows the lowest order QCD diagram where charm quark and anti-charm quark is formed.
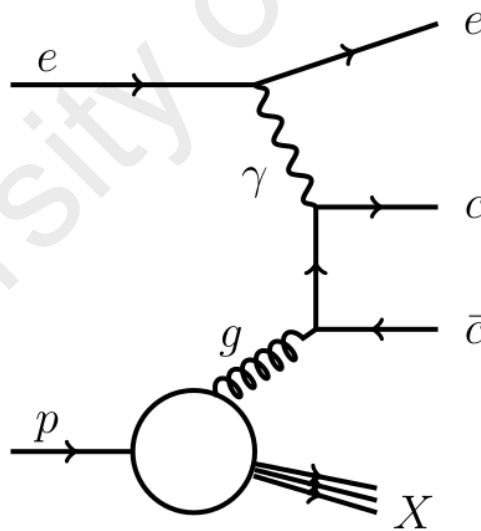
Figure 2.5: Feynmann diagram of charm quark production in e-p scattering.

CHAPTER 3: HERA ACCELERATOR AND ZEUS DETECTOR

3.1 Introduction

This analysis was performed using data collected at the ZEUS detector, one of the four major experiments of the HERA accelerator, which is the first e-p collider in the world. HERA I operated from 1992-2000, and the upgraded machine, HERA II operated from 2002-2007. During the shutdown of HERA in 2000-2001, the luminosity was increased until a factor of 5 from the original luminosity (Adamczyk et al., 2014). ZEUS is a multi-purpose particle detector located at the southern area of HERA ring that measured momentum and energies of particles created during the collision of electron-proton beams. In this chapter, the details of HERA accelerator and components in the ZEUS detector that are relevant to this thesis will be discussed.

3.2 HERA Accelerator

The *Hadron Elektron Ring Anlage (HERA)* (1993) was an accelerator to collide electrons and protons at high energy ($\sqrt{s}$ = 318 GeV) in order to study hadron structure. It was 6.3 km in circumference and 15 to 30 m under ground which is located in Hamburg, Germany. The construction of HERA took place from 1984 until 1990 and started operated in 1992 until 2007. There were four experiment halls placed around the HERA ring as shown in the Figure 3.1 and Figure 3.2. ZEUS (1993) and H1 (Abt et al., 1997) experiments were located at the north and south hall respectively, while at the east and west hall, there were HERMES (Ackerstaff et al., 1998) and HERA-B (HERA-B, 2000) experiment. In ZEUS and H1 experiments, electron proton collision were recorded. It provided information about the process inside the proton that occurred during the collision. HERMES and HERA-B were fixed target experiments where HERMES collided polarised electron beam on polarised gas target to study the spin structure of the nucleon

and HERA-B collided proton beam on aluminium wire target located in the halo of the

proton to study the CP violation in B-meson production (HERA-B, 1995).

Figure 3.1: Overhead view of HERA Accelerator located in Hamburg, Germany (Verena, 2006).
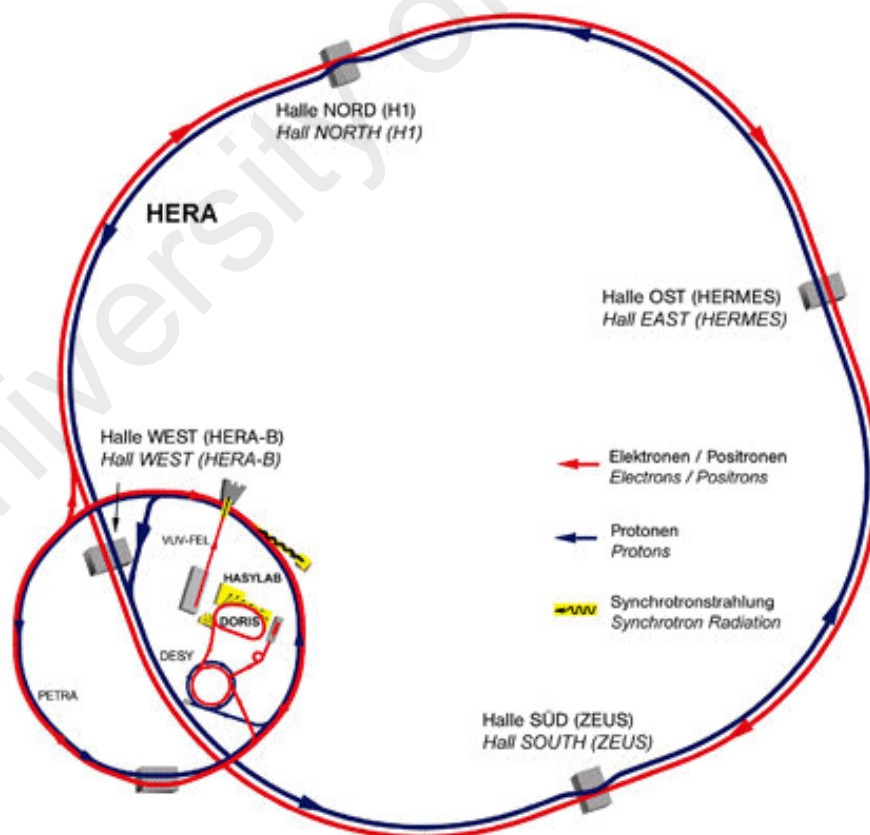
Figure 3.2: ZEUS experiment is conducted at the southern area of HERA ring, where ZEUS detector is situated.

3.2.1 HERA Injection System

The electrons and protons undergo several steps of pre-acceleration in linear and circular accelerators before injected into HERA ring. Pre-acceleration of electrons started in the linear accelerator, LINAC II up to 450 MeV. They were then passed into DESY II and accelerated to an energy of 7.5 GeV. Next, the electrons transferred to PETRA where they were accelerated to 14 GeV and finally injected into HERA where they reached their final energy of 27.5 GeV.
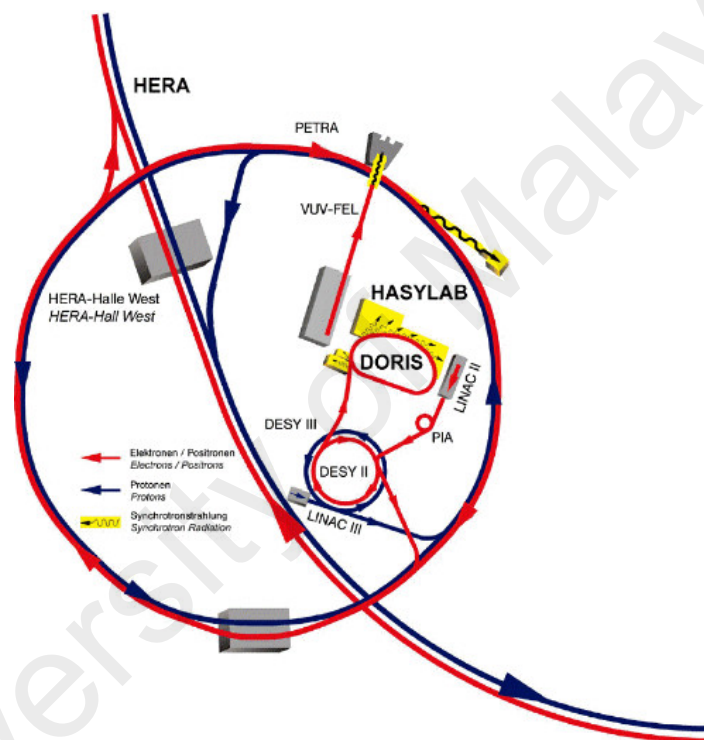
Figure 3.3: Zoom in view of HERA pre-accelerator.

For protons, they where produced by LINAC III and accelerated to 50 MeV by shooting hydrogen ions (H^-) through a thin foil to strip off the electrons. The protons obtained were injected into DESY III, accelerated to 7.5 GeV and then transferred to PETRA where they reached an energy of 40 GeV. Finally, the protons were injected into HERA ring and accelerated to an energy of 920 GeV.

15

3.3 ZEUS Overview

ZEUS is a multi-purpose detector, designed to study various aspect of particle physics during e-p interactions. It has a dimension of $12 \times 10 \times 19$ m^3 weighing of 3600 tons and has almost the entire 4π solid angle coverage.
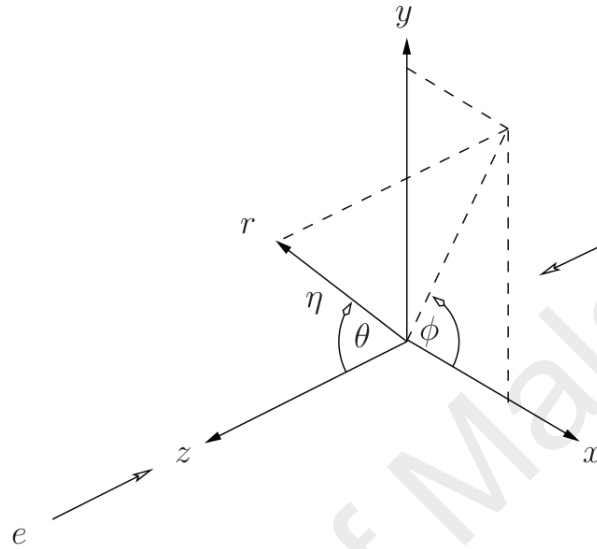
Figure 3.4: ZEUS coordinate system (Whyte, 2008).

ZEUS coordinate system is a right-handed Cartesian system where the origin is at the nominal interaction point. The x-axis points to the center of HERA collider, the y-axis points upwards and the z-axis lies along the proton beam direction. The polar angle, θ, is measured relative to the $+z$-axis which is referred as the forward direction. The azimuthal angle, ϕ, is measured with respect to the x-axis and the pseudorapidity, η, is given by:

$$\eta = -ln(tan\frac{\theta}{2}) \tag{3.1}$$

The following descriptions of ZEUS components are mainly related to this analysis. A full description of ZEUS detector can be found in (ZEUS, 1993).

Figure 3.5: ZEUS detector cross sectional cut.

Figure 3.6: ZEUS detector longitudinal cut. Vertex Detector (VXD) has been replaced by Micro Vertex Detector (MVD) during upgrade of HERA II. The MVD is surrounded by Central Tracking Detector (CTD) which is enclosed by superconducting magnet that produce 1.43 T of magnetic field (Verena, 2006).

17

3.3.1   Central Tracking Detector (CTD)

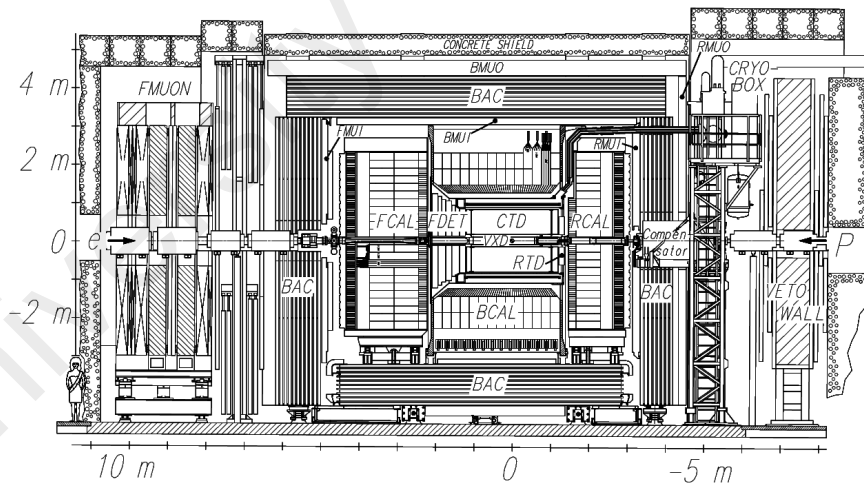CTD (Foster et al., 1994) is the most important component in the ZEUS detector used in this analysis. It was used to detect charged particles and measure their momentum and direction as well as to estimate energy loss, dE/dx which provided information for particle identification. The detector is a cylindrical drift chamber that covered active region along the z-axis from z = -100 cm to z = +104 cm with an inner radius of 18.2 cm and 79.4 cm outer radius, resulting in pseudorapidity coverage of $|\eta|$ < 2. It is filled with gas mixture of argon (Ar), carbon dioxide (CO_2) and ethane (C_2H_6) in the proportion 83:12:5 at atmospheric pressure.

The cylindrical drift chamber made up of 576 cells, each cell has 8 sense wires and they are grouped together in 9 superlayers. The odd numbered superlayers, also called axial layers, had wires parallel to the z direction while even numbered superlayers, the so-called stereo layers had a small angle ($\pm$ 5°) with respect to the beam axis to allow determination of z position accurately. In addition, another way to determine z position is by z-timing system (Foster et al., 1993). The first three axial superlayers are equipped with z-by-timing electronics where the z-position were obtained by measuring the time differences between the signals reaching the two ends of the wire.

The wires in CTD is divided into two categories, 4608 sense wires and 19584 field wires. When a charge particle traverse the drift chamber, it interacts with the gas in the chamber and ionization of gas occurred. The electrons drift towards positive potential sense wire to detect the signal for track reconstruction while the positive ions move towards negative potential field wire to control the electric field inside the detector.

Since CTD is surrounded by superconducting solenoid that provided magnetic field of 1.43 T, it caused charge particles to travel in circular path of radius, R, and this allowed to determine the transverse momentum, p_T of the charged particle based on the relation
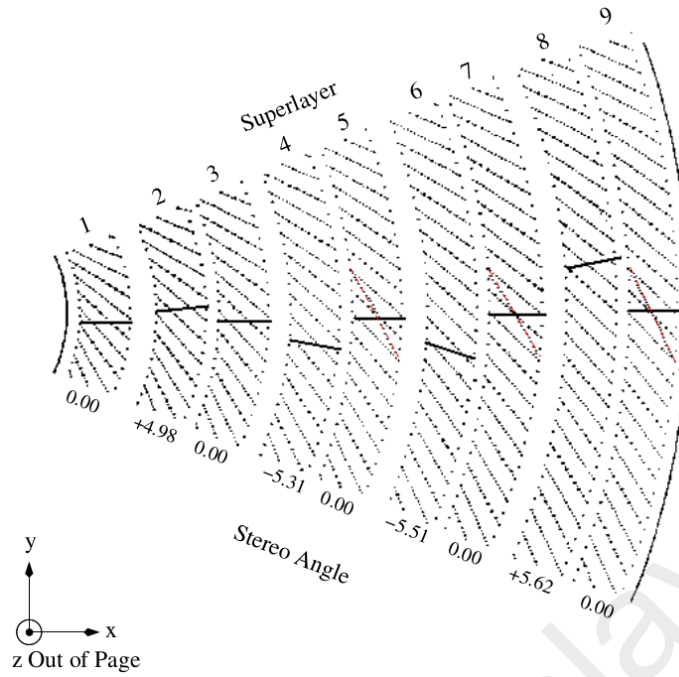
Figure 3.7: CTD cell's cross section with the stereo angles of each superlayer (Whyte, 2008).

of the equation below:

$$R = \frac{p_T}{|q|\,B} \tag{3.2}$$

where $|q|$ is the positive charge of the particle in Coulombs and B is the magnetic field in Tesla. The resolution (Wilton et al., 1999) of transverse momentum for full-length CTD tracks is:

$$\frac{\sigma_T}{p_T} = 0.0058 p_T \oplus 0.0065 \oplus \frac{0.0014}{p_T} \tag{3.3}$$

Here $\oplus$ indicates terms are added in quadrature. The first term corresponds to position resolution, whereas the second and third are due to multiple scattering before and inside the CTD, respectively.

3.3.2 Micro Vertex Detector (MVD)

During HERA shutdown from 2000-2001, Micro Vertex Detector (MVD) (Polini et al., 2007) was installed in ZEUS detector for HERA II upgrade, equipped with a total of

712 silicon strips sensors and it lies closest to the interaction point. The main purpose of MVD is to improve the global momentum precision of the tracking system and to enhance the measurement of short-lived particle of secondary decay vertexes. This helped in the hadron decays studies containing heavy quark such as charm and beauty. MVD is divided into two components, Barrel Micro Vertex Detector (BMVD) that covering the central region and Forward Micro Vertex Detector (FMVD) that covered forward region.

The BMVD was organised in 3 layers of cylinders equipped with 600 silicon strips sensors around the beampipe and covered the polar angle between $30°$ to $150°$. BMVD improved the efficiency of pattern recognition and estimation of the track momentum in trigger phase resulted in $24\,\mu m$ hit resolution. The sensors were placed perpendicular and parallel to beam line like a ladder structure so that $r - \phi$ and $r - z$ position can be measured.

The FMVD contained 112 silicon planes sensors arranged in 4 wheels that extended the acceptance in pseudorapidity up to $\eta = 2.6$. They were mounted back to back that created a sector which is the inner and outer sensor and covered the polar angle to $\theta > 7°$.

3.3.3 Straw Tube Tracker (STT)

Straw Tube Tracker (STT) is a gas drift chamber that covered ZEUS forward region between the polar angles of $5°$ and $25°$. The purpose is to improve the efficiency and purity of the track finding in forward direction. STT (Fourletov, 2004) consist of 48 sectors of two different sizes (24 small and 24 big). Small sector contain 194 straws and big sector contain 266 straws arranged in three layers. The diameter of each straw is 7.5 mm with length between 20 to 102 cm. The gas proportion is 80% Ar and 20% CO_2.
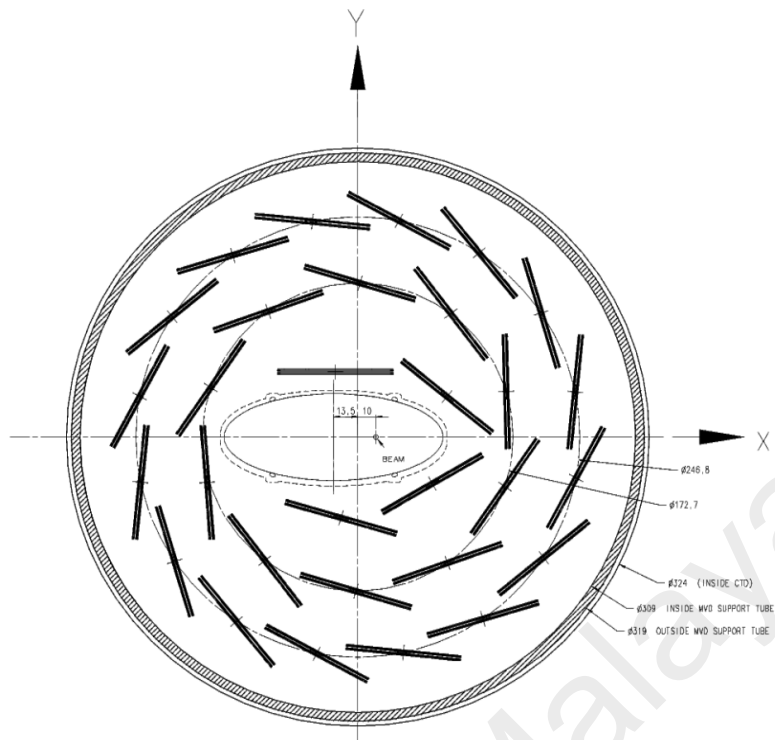
Figure 3.8: A X-Y cut of BMVD. Three layers of cylinders are form in BMVD and the silicon sensors are organised that look like a ladder (Whyte, 2008).
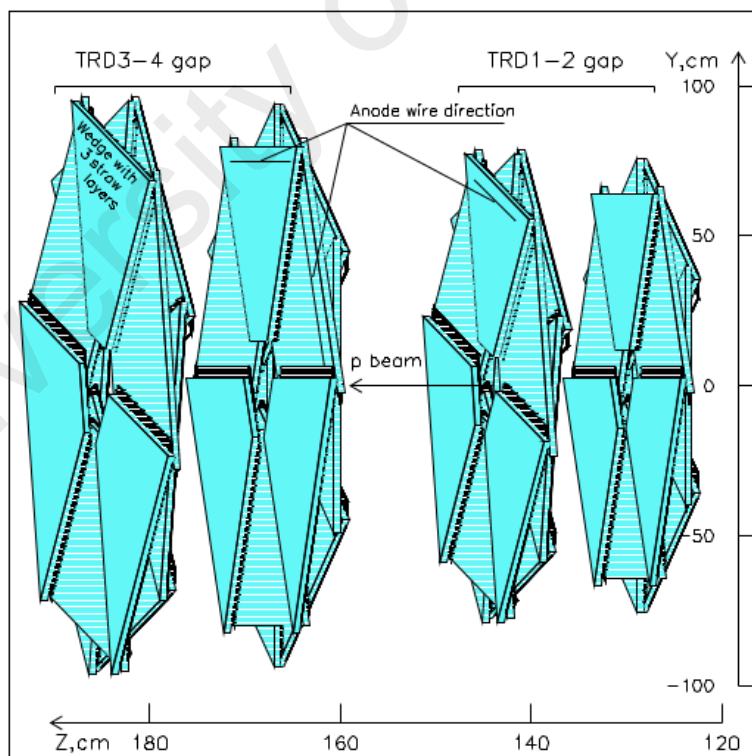
Figure 3.9: STT layout (Roloff, 2011).
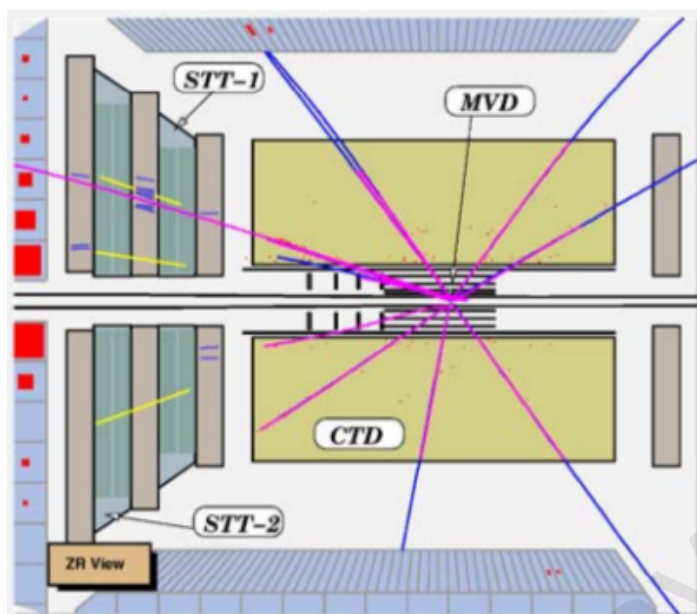
Figure 3.10: Position of STT, CTD and MVD in ZEUS Event Display at ZEUS detector (Fourletov, 2004).

3.3.4   Uranium Scintillator Calorimeter (CAL)

The ZEUS calorimeter, Uranium Scintillator Calorimeter (CAL) (Caldwell et al., 1992) is another important components in ZEUS detector that enclosed the CTD region. It measured the energy deposited from particles that were produced after the e-p collision. The calorimeters consist of 3 regions: Forward Calorimeter (FCAL) (Andresen et al., 1991) with covering angle $2° < \theta < 40°$, Barrel Calorimeter (BCAL) (Derrick et al., 1991) cover $37° < \theta < 129°$ angle and Rear Rear Calorimeter (RCAL) (Andresen et al., 1991) calorimeter with covering angle $128° < \theta < 177°$. Each of these regions are longitudinally subdivided into sections, namely the Electromagnetic Calorimeter (EMC) for inner part and two (one for RCAL) Hadronic Calorimeter (HAC) for outer part. The sections were further divided into cells, that gave the EMC cell size of 5×20 cm^2, the RCAL cell size of 10×20 cm^2 and the HAC cell size of 20×20 cm^2. In total, the CAL contains 5918 cells.

The light produced by a particle when taht passed the cells was collected by plastic wavelength shifter and then transported to the photomultipliers where it is transformed into electrical signals for measurement of each calorimeter cells. The energy resolution for the electrons (hadrons) measured in the test beam were:

$$\frac{\sigma(E)}{E} = \frac{18\% \ (35\%)}{\sqrt{E}} \tag{3.4}$$
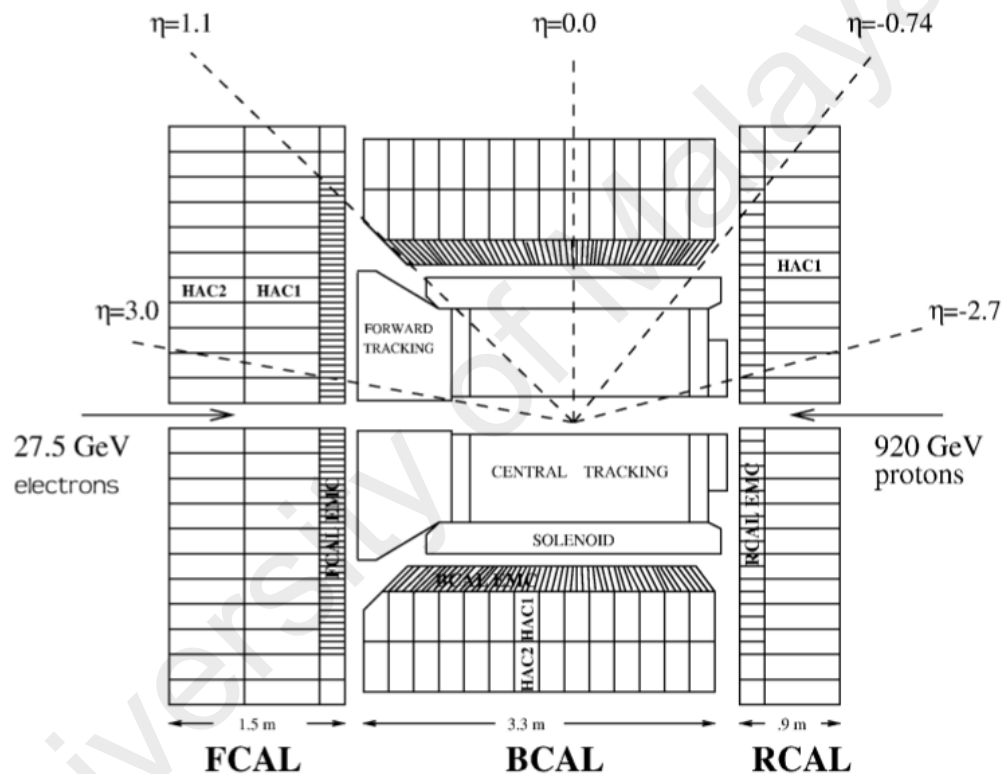
Figure 3.11: Schematic view of ZEUS calorimeter that surround the solenoid and CTD (Grigorescu, 2008).

3.3.5 The Trigger System

The interesting physics events occurred at a small frequency, ~10 Hz, however, the total rate of interaction of e-p collision is 10-100 MHz. Most of the interaction were dominated by non-physics background events mainly caused by the beam gas interaction, cosmic muons passing the CTD and halo muons. Thus, the desire to reduce the rate was

needed and can be achieved by a 3 level trigger system (Smith, Tokushuku, & Wiggers, 1992).

The First Level Trigger (FLT) (Smith et al., 1995) was a hardware trigger, designed to reduce the event rate of up to 1 kHz. Every detector components has its own FLT electronics and since bunch crossings happened every 96 ns, not all detector components can make the trigger decision. Thus, the data are stored in the FLT 4.4 μs pipelines. Detector components stored information like calorimeter energy sums and timing information and passed to the Global First Level Trigger (GFLT). GFLT made a global trigger decision by combining the informations from individual local FLT and made a quick background events rejections. After receiving the decision from GFLT, each pipelines component stopped and the data is sent to the next trigger level.

The Second Level Trigger (SLT) (Uijterwaal, 1992) is a programmable software trigger using INMOS transputer that reduce the rate of event to 100 Hz. Since more time was available in the SLT and sophisticated algorithm was used, it allowed more complex information of the data to be stored like charged particle tracks, vertex determination and calorimeter timing. Similar to GFLT, the Global Second Level Trigger (GSLT) was used to combine all the information from SLT, made a decision and directly sent the data to the Event Builder (EVB) that combine the information from all components and creates data block of a defined format. The data is then further processed to the following trigger level.

Lastly the Third Level Trigger (TLT) (Bailey et al., 1992) is a software trigger that reduces the event rate below 10 Hz and runs offline event reconstruction where physical quantities of the events were calculated. It included better track and vertex finding than SLT. Finally the filtered data were sent to the DESY computing center for the final storage on tapes. This data will then be filtered by event and particle selection of this analysis.

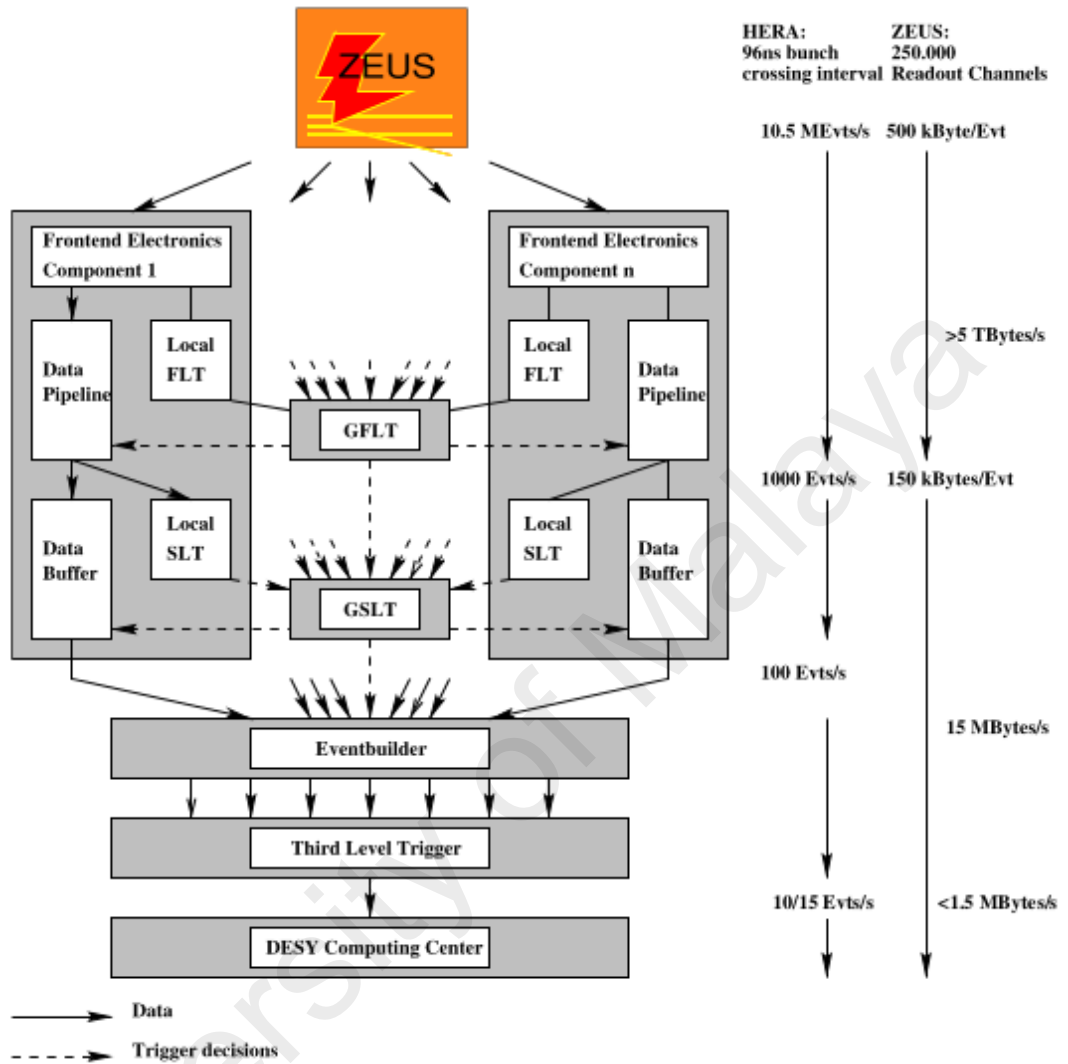An inclusive low-Q^2 triggers was used in this work and the details are described later in this thesis.

Figure 3.12: Work flow of ZEUS three level trigger system (Roloff, 2011).

CHAPTER 4: EVENT RECONSTRUCTION

4.1 Introduction

This chapter will briefly explain about the track reconstruction in the ZEUS detector starting from hits in tracking detector until the fitted tracks. Then hadronic system and electron reconstruction are described. Lastly, several methods used to reconstruct kinematic variables are discussed.

4.2 Track and Vertex Reconstruction

In ZEUS experiment, tracks are trajectories of particles built from hits in the tracking detectors; MVD, CTD and STT. The error on the hit measurement and the effect of multiple scattering were taken into account for the track reconstruction. New improvement of track reconstruction is added since the upgraded of HERA-II and briefly explained in the first sub-section. After the track reconstruction, the primary and secondary vertices were identified and fitted.

4.2.1 Track Finding and Fitting

Firstly, the hit position in each tracking detectors were reconstructed individually using their own software packages. Secondly, a pattern recognition is performed using information from MVD, CTD and STT detectors (Hartner, talk at the ZEUS collaboration meetinga, talk at the ZEUS collaboration meetingb) where a group of hits are combined to form track seeds. The track seeds were started from the outermost layer of the detector, either CTD or STT as it has lower hit density. Then the seeds collected more hits from the inner tracking detectors using an approximate estimation of the momentum and charge of the tracks to connect to the interaction point until a road of hits is formed. Some tracks have only hits in one of the tracking detectors and was stored as CTD-only or MVD-only tracks. There were also tracks that used the information from MVD and CTD as well but

also used the Kalman filter technique (Maddox, ZEUS-03-008 (2003); Fruhwirth, 1987) to improve the track parameter accuracy near the vertex. It is called ZTT tracks.

For track fitting, the output from track finding were used as an input to perform rigorous approach of track fit (Spiridonov, 2008). This approach took into account the magnetic field's inhomogeneity, multiple scattering and energy loss and make use of Kalman filter technique (Maddox, ZEUS-03-008 (2003)). This approach optimized the computations thus making the fitting procedure much faster.

4.2.2 Vertex Finding and Fitting

Firstly, the tracks that belong to the same decay vertex were identified. Then the vertex was fitted by estimating the vertex position and track parameters at the vertex. For the primary vertex, it is reconstructed using VCTRACK (Hartner, ZEUS-98-058 (1998)) package where initially it is assumed that the primary vertex should be lying along the beam line. Then the track pairs that were compatible with a common vertex were combined with the other track pairs. χ^2 fit was performed to determine the vertex position and only the best overall χ^2 were stored. A Deterministic Annealing Filter (DAS) (Fruhwirth & Strandlie, 1999) was used to optimize the precision of the vertex position. For the secondary vertices, it is fitted using the same way but only for the tracks that fulfill these conditions:-

- $p_T > 0.5$ GeV

- At least four hits in the MVD

- At least three hits in the CTD

27

4.3 Hadronic System Reconstruction

ZEUS Unidentified Flow Objects (ZUFOs)[1]is a method that improved hadronic reconstruction by combining calorimeter and tracking information (Tuning, ZEUS-01-021 (2001)). For higher (lower) energy particles, CAL (CTD) gives better energy resolution. Below are the steps for ZUFOs reconstruction.

Firstly, a *cell island* from the calorimeter was formed. Energy cells in EMC, HAC1 and HAC2 were clustered separately and cells that have highest energy deposit were connected with the nearest neighbouring cells to form an island.
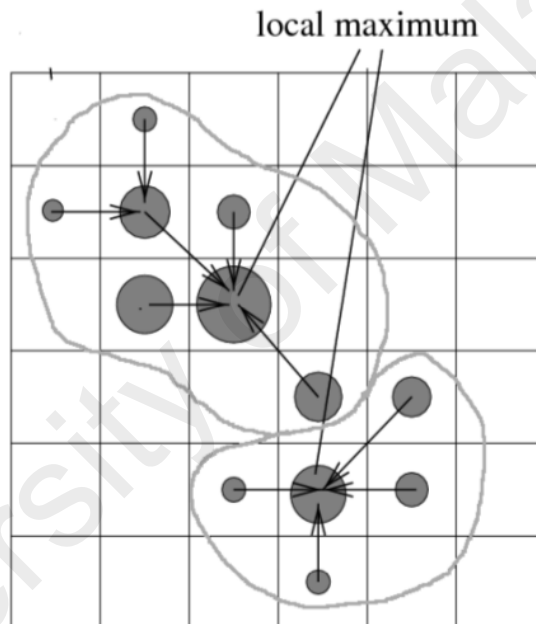
Figure 4.1: Schematic diagram of *cell islands*. The filled circles was the energy deposited in the cells and the different in size shows the different amount of the energy. The gray lines that surround the connected cells were the *cell islands* (Bachynska, 2012).

Secondly, the *cell islands* were clustered in the (θ, ϕ) space to form three dimensional objects called *cone islands*. The angular separation between the cell islands were calculated starting from outermost layer of CAL and goes inward to the beam pipe. The

---

[1]ZUFOs also known as Energy Flow Objects (EFOs) in ZEUS publications
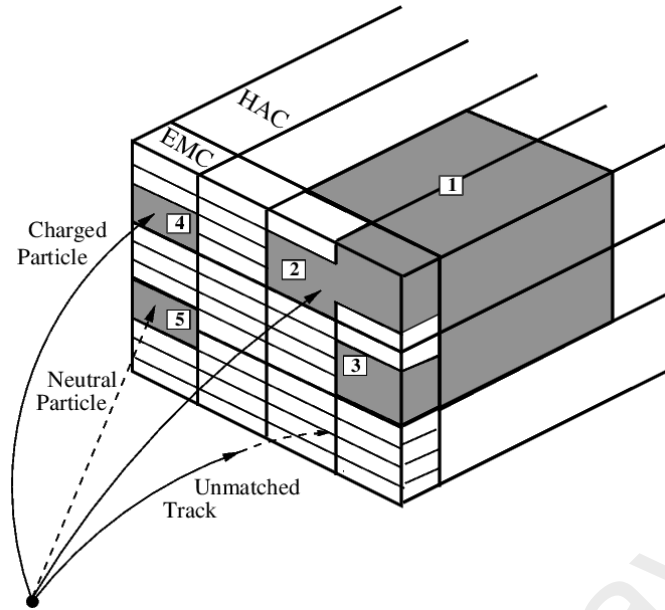
Figure 4.2: Schematic diagram of ZUFOs reconstruction with tracks matched to it. The neighbouring CAL were clustered into *cell islands*. Then EMC *cell islands* labelled 2 and 3 were joined with HAC *cell island* labelled 1 to form a *cone island*. The combined *cone island* and cone island 4 were matched to tracks so they were charge particles, no track was matched to cone island 5 so it is treated as neutral particle and unmatched track correspond to a low momentum particle (Tuning, ZEUS-01-021 (2001)).

position of the cone islands are determined by the logarithmic center of gravity of the CAL shower[2].

Thirdly, tracks were matched to the islands. Tracks that were fitted to the vertex in transverse momentum range $0.1 < p_T < 20$ GeV and passed at least four CTD superlayer were selected for the cone islands (Tuning, ZEUS-01-021 (2001)) matching. Higher transverse momentum range $20 < p_T < 25$ GeV and passed at least seven CTD superlayer were also considered for the matching. The tracks were extrapolated to the inner surface of CAL taking into account the magnetic field. A match was found when the Distance Closest Approach (DCA) between the track and the position of the cone island was less than 20 cm or if the track was located inside the island.

---

[2]The logarithmic energy weight is used instead of linear energy weight to take into account the exponential falloff of the shower energy distribution from the shower maximum.

The CTD information is used if a track matched to a cone island fulfilled these two conditions:

- The track momentum exceeds the energy measured in the CAL, within the resolution of the measured ratio E_{cal}/p:

$$\frac{E_{cal}}{p} < 1.0 + 1.2 \cdot \sigma(\frac{E_{cal}}{p}) \qquad (4.1)$$

where E_{cal} is the energy measured in CAL, p is the track momentum and $\sigma(\frac{E_{cal}}{p})$ is the resolution of the measured ratio E_{cal}/p

- The momentum resolution of the track is smaller than the energy resolution of the associated CAL object:

$$\frac{\sigma(p)}{p} < \frac{\sigma(E_{cal})}{E_{cal}} \qquad (4.2)$$

where $\sigma(p)$ and $\sigma(E_{cal})$ are the measured momentum resolution of track and energy in CAL respectively.

Below are the cases where decisions has been made which energy information to use for one track to one cone island:

- Good tracks that are not matched with cone islands used CTD information to derive the energy by assuming the particle is a pion.

- Cone islands that are not matched with any tracks used CAL information and treated as neutral particles.

- Cone islands that are matched with more than three tracks used CAL information and treated as jets.

The more complicated 1-to-2, 1-to-3, 2-to-1 and 2-to-2 track-island matches are treated similarly as 1-to-1 match, but used the sum of energies in CAL and sum of momentum in CTD. Finally, for case where a track matches with one or two islands and the energy of CAL is favoured, the more precise angular information of the tracks is used.

4.4 Electron Reconstruction

SINISTRA (Abramowicz, Caldwell, & Sinkus, 1995) is a ZEUS software algorithm that reconstruct scattered electron based on neural-network approach. Most of the scattered electron deposited energy in EMC cells and a very small leakage fraction in HAC cells. SINISTRA used the same approach as previous section for the electron identification. The neighbouring cells were grouped into islands and the longitudinal and transverse energy of energy clusters were calculated. The software takes this information as an input and gives the probability of each electromagnetic cluster to be scattered electron as an output. SINISTRA neural network is trained on DIS Monte Carlo samples to simulated the energy clusters in RCAL. Figure 4.3 shows the comparison between hadronic and electromagnetic clusters. The electromagnetic clusters in EMC have high resolution and closest to the interaction point compared to hadronic clusters in HAC. Thus the ratio of electromagnetic over hadronic cluster is closest to one. Only candidates that have more than 0.9 probability is considered as electrons and used for this analysis.

4.5 Kinematic Variables Reconstruction

The total transverse momentum $p_{T,had}$ and angle γ_{had} of the hadronic system as well as energy $E'e$ and polar angle θ_e of the scattered electron are obtained after the reconstruction of the hadronic system and the scattered electron. The equations for hadronic
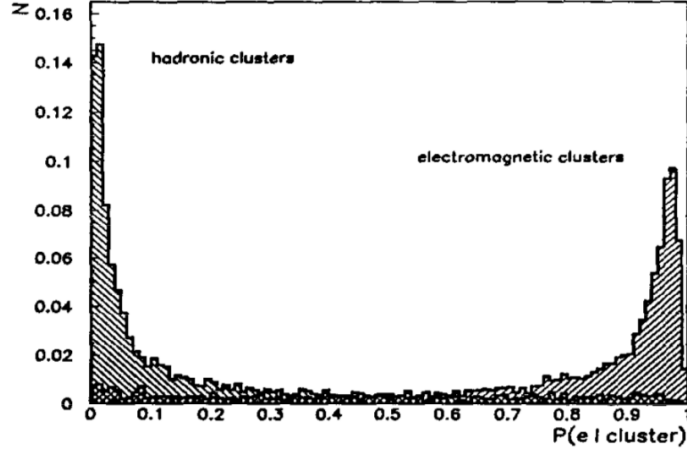
Figure 4.3: Probability distribution for a given cluster to be an electromagnetic cluster $P(e|cluster)$ using SINISTRA.

system are given as:

$$p_{T,had} = \sqrt{\sum_i (p_{x,had}^i)^2 + \sum_i (p_{y,had}^i)^2}$$ (4.3)

$$\gamma_{had} = \frac{\sum_i E_{had}^i \cos\theta^i}{\sum_i E_{had}^i} = \frac{p_{T,had}^2 - \delta_{had}^2}{p_{T,had}^2 + \delta_{had}^2}$$ (4.4)

where $\delta_{had} = E - p_z = \sum_i (E_{had}^i - p_{z,had}^i)$. The sum runs over all particles in hadronic state except the scattered electron. These variables are used to reconstruct kinematic variables Q^2, x and y. Different methods are chose for different kinematic regions but it is also possible to combine the different methods for the optimization of the kinematics reconstruction. The three main methods in ZEUS are described below.

4.5.1 Electron Method

This method used only information of energy $E'e$ and angle θ_e of the scattered electron (Bentvelsen et al., 1992). The kinematics variables of this method are:

$$Q_{el}^2 = 2E_e E_e'(1 + \cos\theta_e)$$ (4.5)

$$x_{el} = \frac{Q_{el}^2}{s y_{el}} \tag{4.6}$$

$$y_{el} = 1 - \frac{E_e'}{2E_e}(1 - \cos\theta_e) \tag{4.7}$$

where E_e is the energy of the incoming electron and s is the e-p center of mass energy. This method give better resolution at low Q^2.

4.5.2 JB Method

This method used only information of variables from the hadronic system (Jacquet & Blondel, U. Amaldi (ed.), p. 391. Hamburg, Germany (1979). Also preprint DESY 79/48). Since this method can be used even if the scattered electron is not measured, CC DIS process and PHP process are also used this method. The kinematic variables are as follow:

$$Q_{JB}^2 = \frac{p_{T,had}}{1 - y_{JB}} \tag{4.8}$$

$$x_{JB} = \frac{Q_{JB}^2}{s y_{JB}} \tag{4.9}$$

$$y_{JB} = \frac{\delta_{had}}{2E_e} \tag{4.10}$$

4.5.3 DA Method

This method used information of angle θ_e of the scattering electron and angle γ_{had} of the hadronic system (Bentvelsen et al., 1992). Usually angles are measured more precisely than energies in ZEUS detector, so this method allowed more precise measurement

of kinematics in a large fraction of the phase space. The kinematics variables are given as:

$$Q_{DA}^2 = 4E_e^2 \frac{\sin\gamma_{had}(1 + \cos\theta_e)}{\sin\gamma_{had} + \sin\theta_e - \sin(\gamma_{had} + \theta_e)} \tag{4.11}$$

$$x_{DA} = \frac{E_e}{E_p} \frac{\sin\gamma_{had} + \sin\theta_e + \sin(\theta_e + \gamma_{had})}{\sin\gamma_{had} + \sin\theta_e - \sin(\theta_e + \gamma_{had})} \tag{4.12}$$

$$y_{DA} = \frac{\sin\theta_e(1 - \cos\gamma_{had})}{\sin\gamma_{had} + \sin\theta_e - \sin(\theta_e + \gamma_{had})} \tag{4.13}$$

where E_p is the energy of incoming proton. Contrary from the electron method, this method gives better resolution at high Q^2.

CHAPTER 5: EVENT AND D$^+$ SELECTION

5.1 Introduction

This chapter will firstly explain about the type of Monte Carlo (MC) and data samples used for this analysis. Then, event selection criteria will be discussed which consist of trigger and DIS selection. A few triggers from FLT and SLT are described and the standard trigger for TLT; SPP02, SPP09, HFL17 and HPP31 are used to select NC DIS events. The events that are triggered will pass through the DIS event selection where at this stage, most of the PHP events are rejected. Lastly, box cut and geometry cuts are applied to select only good reconstructed scattered electron. This chapter ends with the selection of D$^\pm$ candidates which will then be measured in the next chapter.

5.2 Monte Carlo and Data Samples

Simulated events were generated using MC method which is described in reference (Metropolis & Ulam, 1949; Weinzierl, 2000). They were simulated based on the various possible physical processes in order to check the detector response by determining the efficiency and acceptance on the model's prediction. The MC generator used for this analysis is Rapidity Gap between Jets (RAPGAP).

RAPGAP (Jung, 1995) is an event generator used to simulate charm and beauty production in DIS. RAPGAP can be either diffractive or non-diffractive depending on which MC samples selected. The luminosity of simulated events are described in the table below. Table 5.1 shows the MC information used for the inclusive D$^+$. The Q^2_{MC} in RAPGAP c inclusive is split into two regions because of Q^2 dependence of the charm cross section. Table 5.2 is an additional MC information used for exclusive D$^+$.

Table 5.1: Non-diffractive MC samples for each year.

MC type	Kinematic region, Q^2_{MC}	Integrated Luminosity, $\mathcal{L}$ (pb^{-1})			
		2003/2004	2005	2006	2006/2007
RAPGAP c inclusive	$1.5 < Q^2_{MC} < 4$ GeV^2	41	148	43	142
	$Q^2_{MC} > 4$ GeV^2	124	283	169	497
RAPGAP b inclusive	$Q^2_{MC} > 1$ GeV^2	1097	2115	925	2578

Table 5.2: Diffractive MC samples for each year.

Year	Beam	Integrated Luminosity, $\mathcal{L}$ (pb^{-1})
2003/2004	e$^+$p	184.8
2005	e$^-$p	539.6
2006	e$^-$p	220.4
2006/2007	e$^+$p	655.2

Table 5.3: Data samples for each year.

| Year	Beam	Integrated Luminosity, $\mathcal{L}$ (pb^{-1})
2003/2004	e$^+$p	36
2005	e$^-$p	134
2006	e$^-$p	53
2006/2007	e$^+$p	137

Table 5.3 shows the full data samples version 08 collected by the ZEUS detector with the center of mass energy of 318 GeV. The total luminosity of the data taking period from 2003-2007 is 360 pb^{-1}.

At low Q^2 either e$^+$p or e$^-$p beams can be used as NC DIS cross sections are invariant with respect to the lepton charge, within the phase space applicable to this analysis, as demonstrated in Figure 5.1 (Abramowicz et al., 2015)

5.3 Trigger Selection

In FLT, only a very short decision time is available to select events from e-p collision hence only general background rejection and preliminary scattered electron reconstruction are implemented. The cuts are based on information from CAL, CTD and vetos from detectors. A combination of FLT slots compatible with signal topology is used to select
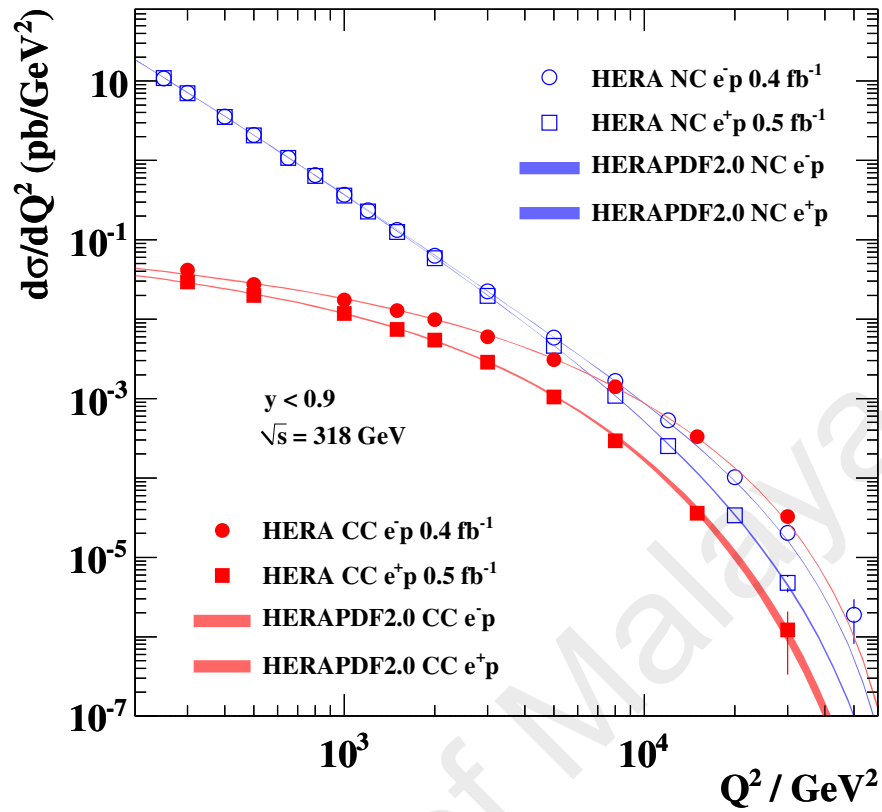
Figure 5.1: The cross section of HERA NC and HERA CC versus momentum transfer-squared, Q^2. The blue circle and square is the HERA NC in e^-p and e^+p beam respectively. Notice that the contribution from NC interaction mediated by Z becomes important only at high Q^2, which explain the divergence between e^-p and e^+p cross section. Since the upper limit Q^2 used in this analysis is 1000 GeV^2 (see section 5.4), only interaction mediated by photon dominates, which is invariant with respect to lepton charge (Abramowicz et al., 2015). The red and blue thick lines are the theoretical uncertainty. The thicker the line, the larger the uncertainty.

events at this level.

The events that passed the FLT is sent to the SLT Soft Photoproduction (SPP1) slot. Since more decision time is available at SLT, a more complex physics quantities can be calculated such as energy momentum transfer (E - p_z).

Finally, the NC DIS events are selected by TLT. The TLT slots used for this analysis are briefly described as follow (Lisovyi, 2011). Notice that each events only need to pass

at least one of these slots[1] and the values of the criteria are the preselection cuts decided by the trigger in ZEUS experiment.

- SPP02[2]. It is an inclusive low-Q^2 trigger with small box cut[3] and valid for 2004 and 2005. The criteria required are:

  - $30 < E - p_z < 100$ GeV

  - $E'_e > 4$ GeV

  - small box cut: $|x| > 12$ cm, $|y| > 12$ cm

- SPP09. It is an inclusive low-Q^2 trigger with medium box cut and valid since 2006. The criteria are:

  - $30 < E - p_z < 100$ GeV

  - $E'_e > 4$ GeV

  - medium box cut: $|x| > 15$ cm, $|y| > 15$ cm

- HFL17[4]. It is an inclusive NC DIS and valid since 2006. It has the same selection as in SPP02 plus an additional requirement of 2 TLT tracks in CTD.

- HPP31[5]. It is an inclusive low-Q^2 trigger with small box cut and valid since 2006. The criteria are:

  - $34 < E - p_z < 75$ GeV

  - $E'_e > 7$ GeV

---

[1]The slots are named according to the physics group they were originally intended for and the number beside the slots are the bits

[2]SPP is the abbreviation for soft photoproduction

[3]The box cut is the position of scattered electrons in RCAL that required to be outside a box (some region in CAL) around beam pipe

[4]HFL is the abbreviation for heavy flavour

[5]HPP is the abbreviation for heavy photoproduction

– $Q^2_{TLT} > 6 \text{ GeV}^2$

– 1 track in CTD with $p_T > 0.2$ GeV

– a vertex in an event with $-60 < z_{vtx} < 60$ cm

– small box cut: $|x| > 12$ cm, $|y| > 12$ cm

5.4 DIS Selection

The NC DIS events were selected by implementing the following offline cuts (Abt et al., 2013; Lisovyi, 2011):

- $E'_e > 10$ GeV, where E'_e is the energy of reconstructed scattered electron. This cut increases the purity of DIS electron candidates by reducing the PHP events.

- $E^{cone}_{none'} < 5$ GeV, where $E^{cone}_{none'}$ is the energy deposited in CAL in a cone centered around the electron candidate and not originating from it. The energy calculated in the cone with radius 0.8 cm (ΔR) in the η, ϕ plane is defined as $\sqrt{\Delta\eta^2 + \Delta\phi^2} < 0.8$, where ϕ is the azimuthal angle.

- $40 < E - p_z < 65$ GeV, where $E - p_z = \sum_i E_i(1 - \cos\theta_i)$ and E_i and θ_i are the energy and polar angle of the ith ZUFO candidates. In order to select ideal NC DIS events, $E - p_z$ should be equal to $2\,E_e = 55$ GeV where the $2\,E_e$ is the difference between the total energy of an event before collision ($E = E_p + E_e$) and total longitudinal momentum component ($p_z \approx E_p - E_e$). The lower cut is imposed to suppress PHP events as the value of $E - p_z$ in PHP events is much lower. The upper cut is introduced to reject events caused by cosmic-ray particle.

- $|z_{vtx}| < 30$ cm, where z_{vtx} is the z position of the primary vertex. This cut reduced the beam-gas interaction events and cosmic ray events.

- $y_{JB} > 0.02$, where y is reconstructed using JB method to reject events where the hadronic system is not measured precisely.

- $5 < Q^2_{DA} < 1000$ GeV^2 and $0.02 < y_{DA} < 0.7$, where the kinematic variable Q^2 and y was reconstructed using DA method.

- SINISTRA scattered electron probability > 0.9 to ensure high purity of electron candidate.

5.5 Box Cut and Geometry Cut

The box cut in offline version of SINISTRA is the cut applied to scattered electron position on the CAL surface and the cut is slightly tighter compared to SPP02, HFL17 and HPP31 but looser than SPP09: $|x| > 13$ cm, $|y| > 13$ cm. The geometry cut is the cut removing the CAL region due to the poor reconstruction of scattered electron (Lisovyi, 2011). Below are the geometry cuts where the CAL region is rejected:

- Scattered electrons that overlap between region RCAL and BCAL: $\sqrt{x^2 + y^2} > 175$ cm.

- Scattered electrons in crack region of RCAL, BCAL and FCAL so-called super-cracks: $164 < z < 174$ cm in the positive region, $-104 < z < -98.5$ cm in the negative region.

- The gap between RCAL region: if $y > 0$ cm, $6.5 < x < 12$ cm, if $y < 0$ cm, $-14 < x < -8.5$ cm.

- Cut in RCAL region where cooling tubes and supply cables for the solenoid were mounted: if $y > 80$ cm, $|x| < 12$ cm.

5.6 D⁺ Selection

The decay channel used to reconstruct the D⁺ mesons is $D^+ \rightarrow K^-\pi^+\pi^+$ with branching ratio 9.46 ± 0.24 %. The daughters of D⁺ candidates consist of three tracks where two of them have the same charge and were assigned as pions while the other track is with the opposite charge and is assigned as a kaon. These three tracks were required to come from the same vertex and finally the invariant mass, $M_{K\pi\pi}$ was calculated (Abt et al., 2013). The selection criteria below are applied for the D⁺ candidate reconstruction (Chekanov et al., 2009; Lisovyi, 2011).

- Track quality cuts to ensure high momentum and position resolution:

    - Each track should pass at least three CTD superlayers.

    - Each track should pass at least two BMVD hits; rϕ and rz hits in the xy plane and z direction respectively.

    - Track pseudorapidity, $|\eta_{K\pi}| < 1.75$.

- Track transverse momenta, $p_T^K > 0.5$ GeV and $p_T^\pi > 0.35$ GeV are required to reduce the background.

- The transverse momentum of D⁺, $1.5 < p_T^D < 15$ GeV. At the lower limit, this kinematic region will prevent the increase of background contamination as the acceptance drops quickly to zero. At the upper limit, the cross section is acceptable to be measured with the luminosity.

- The pseudorapidity of D⁺, $|\eta_D| < 1.6$.

There were also some crucial cuts implemented that contribute to the improvement of D⁺ reconstruction. It is described as follow:

- Reflection subtraction of $D^{*+} \rightarrow D^0\pi^+ \rightarrow K^-\pi^+\pi^+$ is applied to suppress the additional peak in the mass spectrum at 2010 MeV by rejecting the mass difference of $0.143 < M_{K\pi\pi} - M_{K\pi} < 0.148$ GeV.

- Reflection subtraction of $D_s^+ \rightarrow \phi\pi^+ \rightarrow K^-K^+\pi^+$ is applied to suppress the asymmetric peak in the mass spectrum. This is performed by treating one of the pion track as a kaon and rejecting events with $1.0115 < M_{KK} < 1.0275$ GeV.

- Decay length significance, $S_l > 4$. This selection improved the sensitivity to $D^+ \rightarrow K^-\pi^+\pi^+$ particles which have longer lifetime compared to most background processes. S_l is defined as the projected decay length on particle's flight direction divided by the error of this projection (uncertainty):

$$S_l = \frac{l_{XY}}{\sigma_l} \tag{5.1}$$

where the l_{XY} is given as:

$$l_{XY} = \frac{\vec{r}_{XY} \cdot \vec{p}_T}{|\vec{p}_T|} \tag{5.2}$$

$\vec{r}_{XY}$ is the 2D position vector from the reference point of interaction to the secondary vertex. The reference point of interaction is not the beamspot itself but instead a reduced DAF vertex with beam constraint, which was used because of the better spatial resolution. The illustration is shown in Figure 5.2.

The uncertainty of the projection is defined as:

$$\sigma_l = \sqrt{(\sigma_{secvtx}^{projected})^2 + (\sigma_{primvtx}^{projected})^2} \tag{5.3}$$

where $\sigma_{secvtx}^{projected}$ and $\sigma_{primvtx}^{projected}$ are the uncertainties of secondary and primary vertices projections respectively.
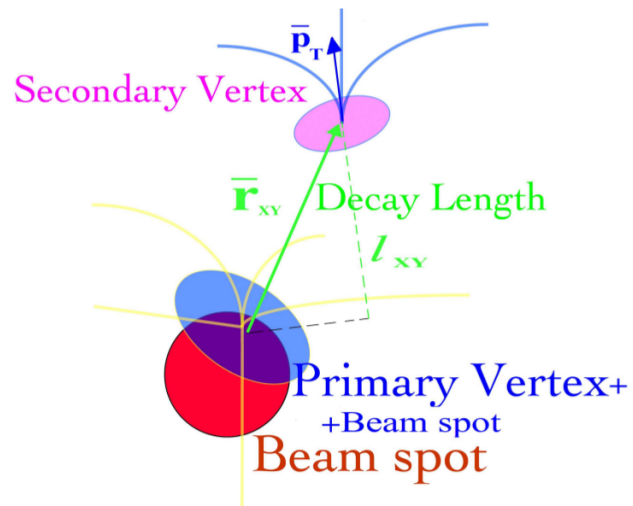
**Figure 5.2:** An illustration explaining the concept of the decay length significance (Lisovyi, 2011).

# CHAPTER 6: INCLUSIVE AND QUASI-EXCLUSIVE D^+

6.1 Introduction

This chapter shows the results of the analysis. At first, we will see the effect of reflection subtraction and significance cuts on the mass of inclusive D^+. Then, the mass of inclusive D^+ meson for full data sample is reproduced and compared with the D^+ ZEUS published paper. The analysis is continued by implementing exclusive cut. Lastly, a different MC sample is used and their description of the data is compared.

6.2 Inclusive D^+

This result shows the relative difference of reflection subtraction and significance cuts as mentioned in previous chapter. This comparison was conducted using data (Table 5.3) and non-diffractive MC samples from 2005 only.
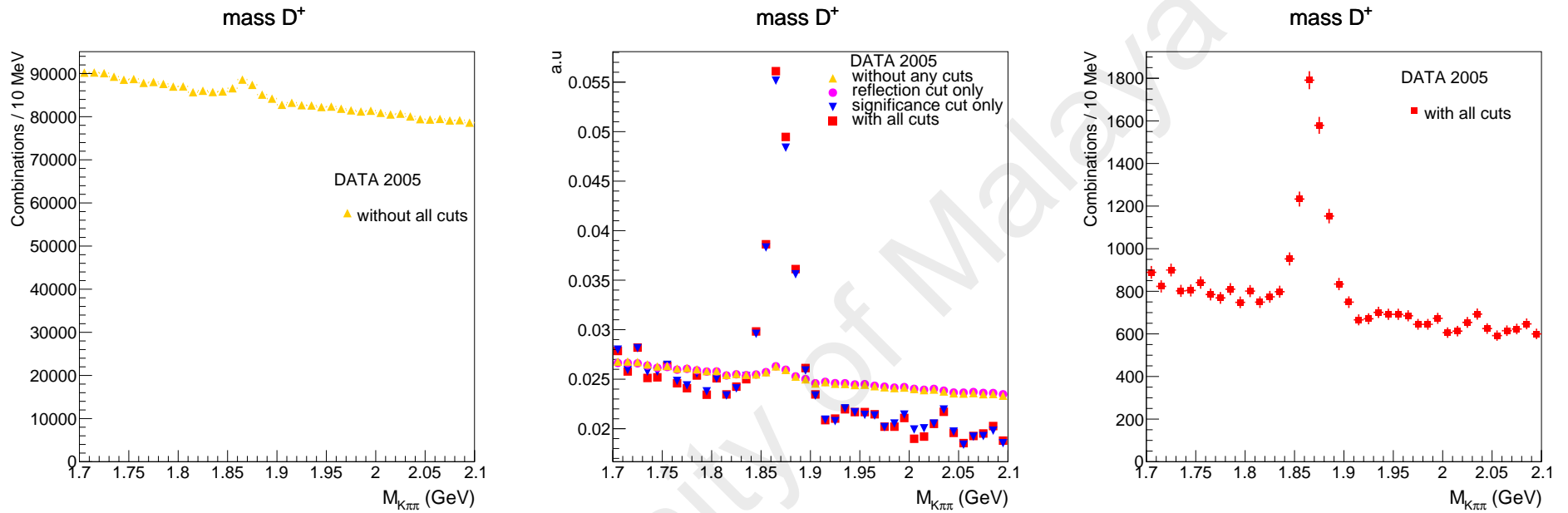
Figure 6.1: Relative difference between reflection subtraction and significance cuts in data. The left and right plots show the mass distribution without and with the cuts respectively. The middle plot is normalized to 1 and provide an additional information of the effect of each cuts.
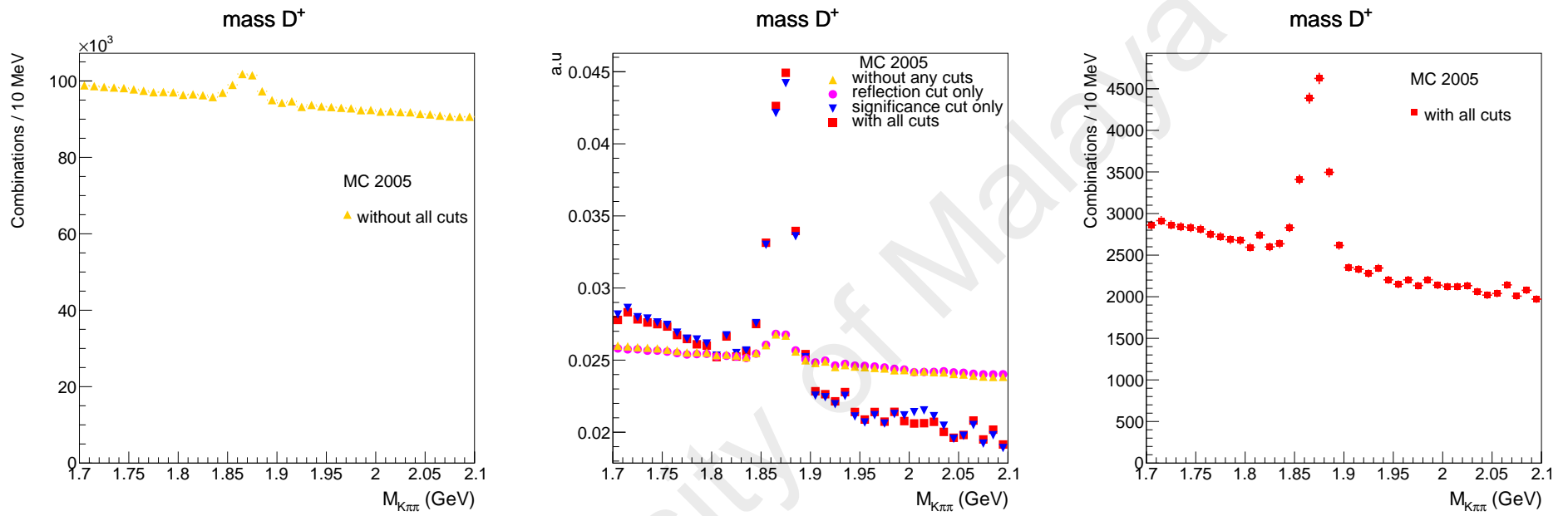
Figure 6.2: Relative difference between reflection subtraction and significance cuts in MC. The left and right plots show the mass distribution without and with the cuts respectively. The middle plot is normalized to 1 and provide an additional information of the effect of each cuts.

6.2.1 Comparison with previous ZEUS paper

The full dataset of inclusive D^+ is analysed to compare with the ZEUS D^+ published paper (Abt et al., 2013) as shown in Figure 6.3 and 6.4. It can be seen that the result is compatible with the paper. This means the analysis at this point is on the right track.
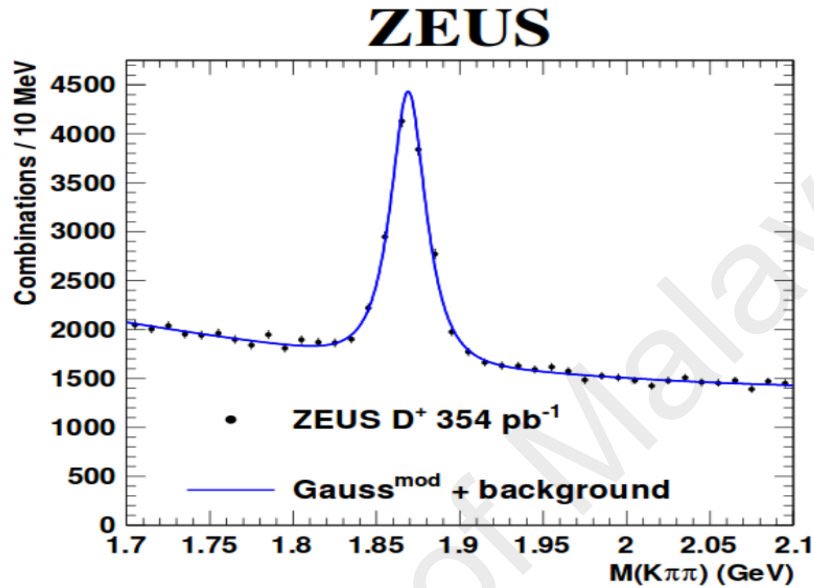
Figure 6.3: ZEUS inclusive D^+ paper with measured mass 1.86897 ± 0.00026 GeV (Abt et al., 2013).
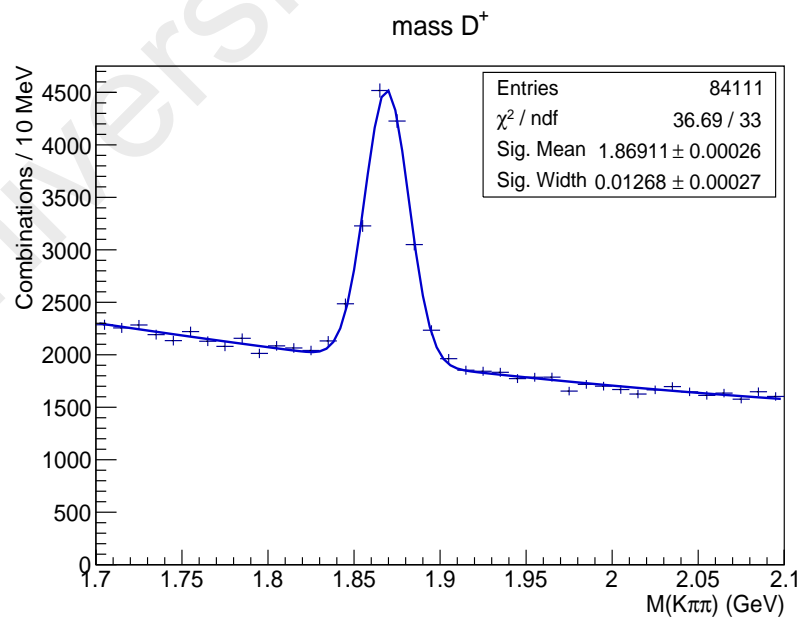
Figure 6.4: Reproduced inclusive D^+ mass distribution with measured mass 1.86911 ± 0.00026 GeV.

6.2.2 Cross section of inclusive D$^+$

The formula of the total cross section is defined as:

$$\sigma = \frac{N_{sig}^{fit}}{\epsilon_{tot}\mathcal{L}\mathcal{B}} \tag{6.1}$$

where $\mathcal{B} = 9.46 \pm 0.24\ \%$, $\mathcal{L} = 360\ \text{pb}^{-}1$ total efficiency , ϵ_{tot} is given as:

$$\epsilon_{tot} = \frac{\epsilon_{MC1.5} + \epsilon_{MC4} + \epsilon_{MC1}}{\mathcal{L}_{MC1.5} + \mathcal{L}_{MC4} + \mathcal{L}_{MC1}} \tag{6.2}$$

and each efficiency is calculated by:

$$\epsilon_{indiv} = \frac{N_{MC}^{reco}}{N_{MC}^{true}} \times \mathcal{L}_{indiv} \tag{6.3}$$

The N_{MC}^{true} is obtained from the matching of the D$^+ \to$ K$^-\pi^+\pi^+$ from the MC true level and N_{MC}^{reco} is the number of these events that passed the analysis cuts. Since the MC have three different ranges of Q^2 (Table 5.1), each of the efficiency is required to multiply with their individual MC luminosity. The N_{sig}^{fit} is the number of D$^+$ signal from the fit minus the number of reconstructed events in b inclusive, $\mathcal{L}$ is the total luminosity of the data (Table 5.3), and $\mathcal{B}$ is the branching ratio of D$^+$ decay to K$^-\pi^+\pi^+$ (Beringer et al., 2012).

The cross section calculated for the inclusive D$^+$ is 4.9 ± 0.2 nb which is consistent with the paper (Abt et al., 2013).

6.3 Quasi-exclusive D$^+$

The analysis was continued by searching for exclusive D$^+$ to achieve our second objective. In our case, this means searching for events where a D$^+$ is produced and nothing else. Exclusive D$^+$ used the same samples and cuts as the inclusive D$^+$ with an additional

cut which is exclusive cut. This exclusive cut required events with only three or four tracks where the three tracks are the tracks of the daughter particles ($K^-\pi^+\pi^+$) and the additional track is the track of the scattered electron track if it is in the tracking acceptance.
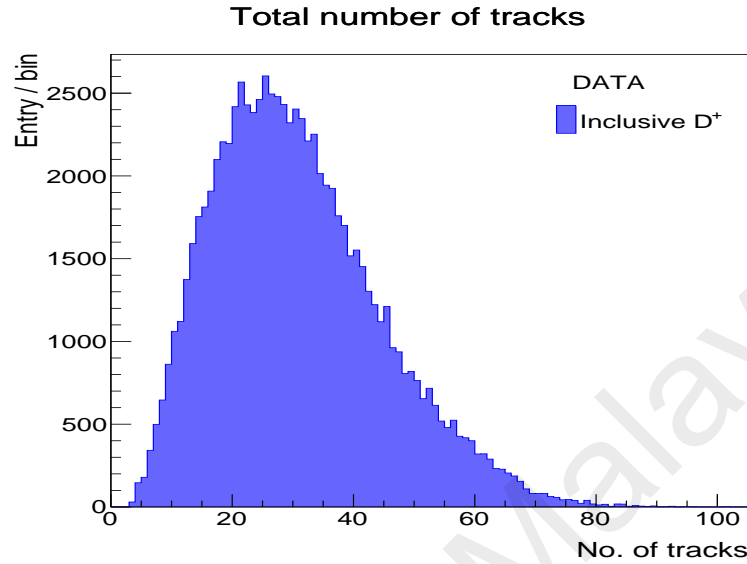
Figure 6.5: Total number of tracks of inclusive D^+ in data.
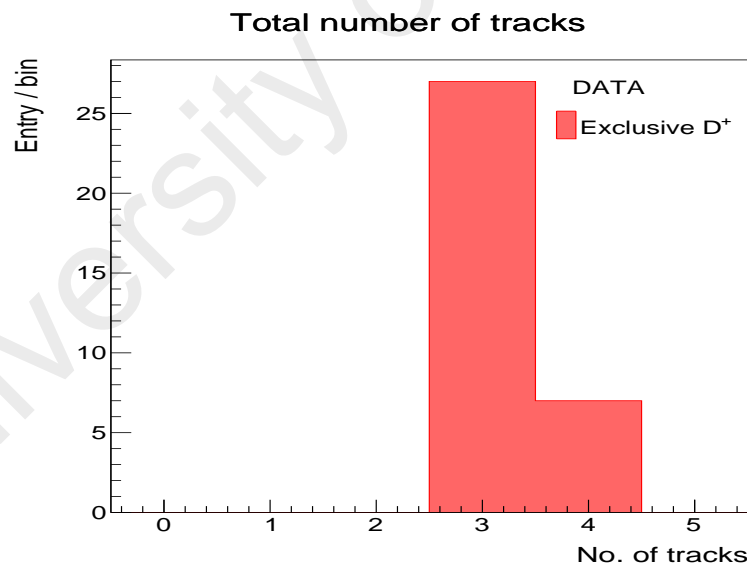
Figure 6.6: Total number of tracks of exclusive D^+ in data.

The Figure 6.5 and 6.6 show the difference on the number of tracks before and after the exclusive cut is implemented. It can be seen in the exclusive D^+ where events with more than three or four tracks are rejected and most of the events consist of three tracks

than four tracks.

Figure 6.5 shows the illustration of a MC event passing the full exclusive event selection. There are only three tracks in the event. The two red lines represent the two pions and the grey line represents a kaon. However, there were also small other activities that happen in the very forward region which was why this event was considered as quasi-exclusive.

Figure 6.7: The most similar illustration to exclusive D^+. The figure is taken from this analysis in MC using ZEVis software.

6.3.1   Scattered Electron

For events that have four tracks, the scattered electron track have to be determined. Firstly, the scattered electron is said to be in the range of track acceptance by fulfilling one of these two conditions:

- If $0.3° < \theta < 2.6°$, the momentum of SINISTRA track > 5 GeV and DCA < 10 cm.

- If outside of this θ range, E - P_z > 44 GeV.

Then the scattered electron track is identified by ΔR matching between the electron and the closest track position where the cone size should be less than 0.074 cm.

6.3.2   Additional MC

For exclusive D$^+$, a different MC, RAPGAP diffractive D meson was added to see which MC describes the data better. This is because the exclusive D$^+$ was unexpected to be observed in ZEUS experiment so there was no dedicated MC to describe the exclusive charm production. The difference between this MC and the previous MC (see Section 5.2) is the process involved; either diffractive or non-diffractive respectively. Besides, the diffractive MC was generated with a preselection of $p_T^{D^\pm} > 2.8$ GeV. The results to follow will show the comparison of data with non-diffractive and diffractive MC as well as the combination of both MC normalized to data.
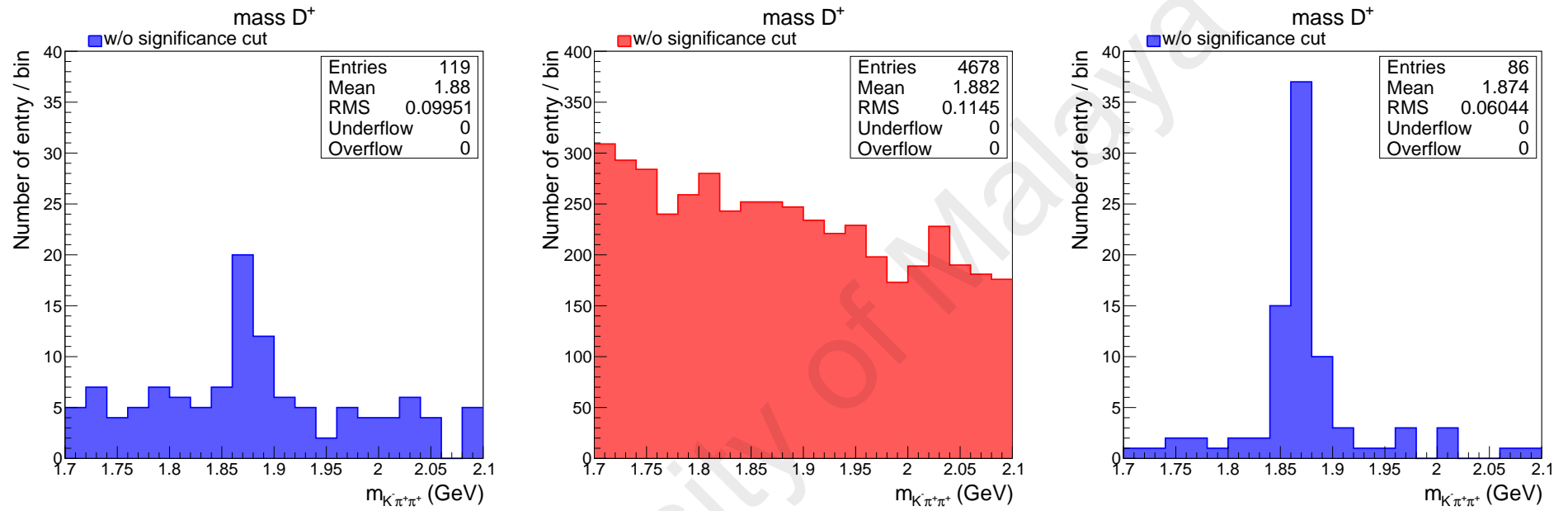
Figure 6.8: Comparison between non-diffractive MC (left), data (middle) and diffractive MC (right) without decay length significance cut in full data and MC samples. Both events in MC show the peak of mass D^+ (1.8696 GeV) while the peak in data is not visible due to the background.
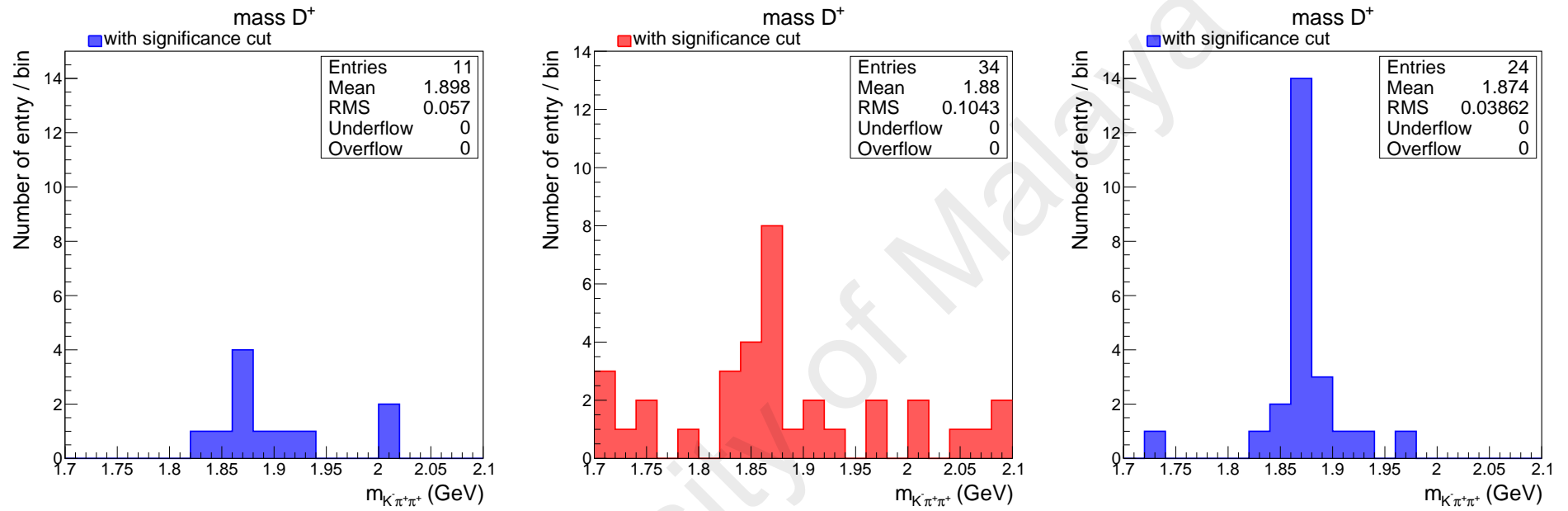
Figure 6.9: Comparison between non-diffractive MC (left), data (middle) and diffractive MC (right) with decay length significance cut in full data and MC samples. D^+ peak is visible in all three histograms.

6.3.3 Combination of MC

In Figure 6.7, it can be seen that events in both MC and data have D^+ signal. However, none of the MC is able to accurately describe the behaviour of the data due to lack of statistics. Therefore, qualitative research is conducted in this analysis to understand the exclusive D^+. First, the combination of MC with a mass cut is done to find the relative contribution of diffractive and non-diffractive MC is needed to describe the data within the mass range, $1.84 < M_{K^\mp \pi^\pm \pi^\pm} < 1.9$ GeV. The ratio of these MC compared to data is carried out from 0.1 to 0.9 and vice versa as shown in Figure 6.8. It can be seen that the rough estimate for the fraction of events from non-diffractive and diffractive mixture is 0.5 ± 0.2. The combined MC with ratio 0.5:0.5 is chosen in plot and compared with each individual MC.
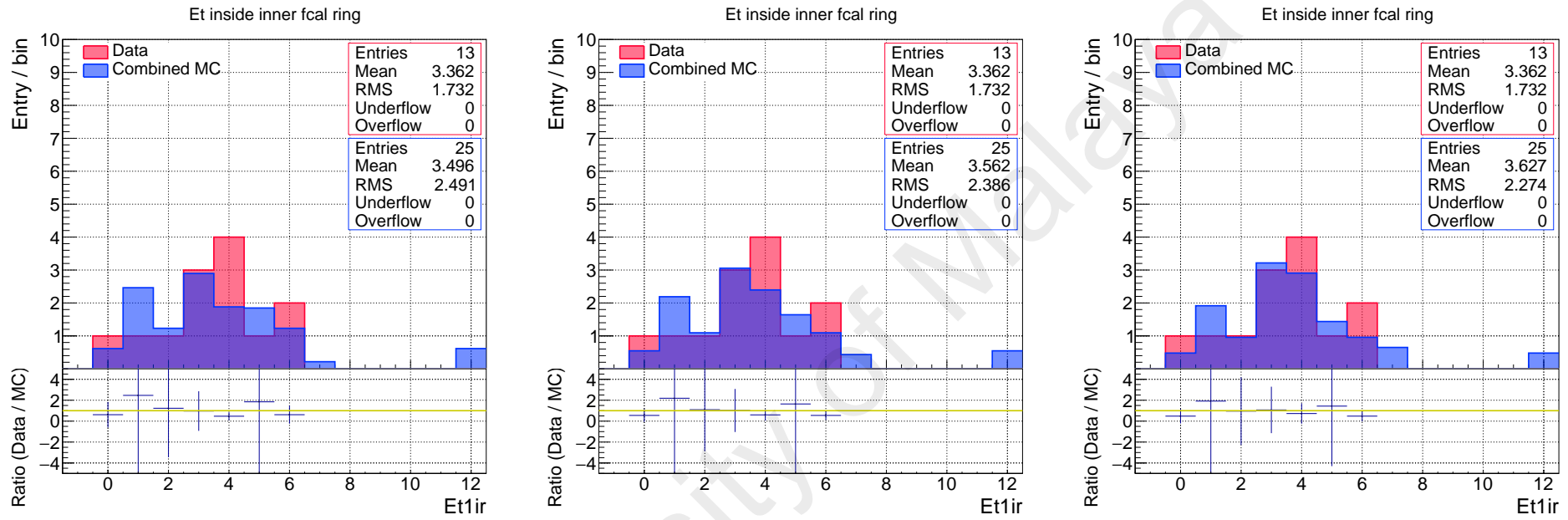
Figure 6.10: Comparison of data and combined MC of transverse energy variable for ratio 0.1:0.9 (left), 0.2:0.8 (middle), 0.3:0.7 (right).
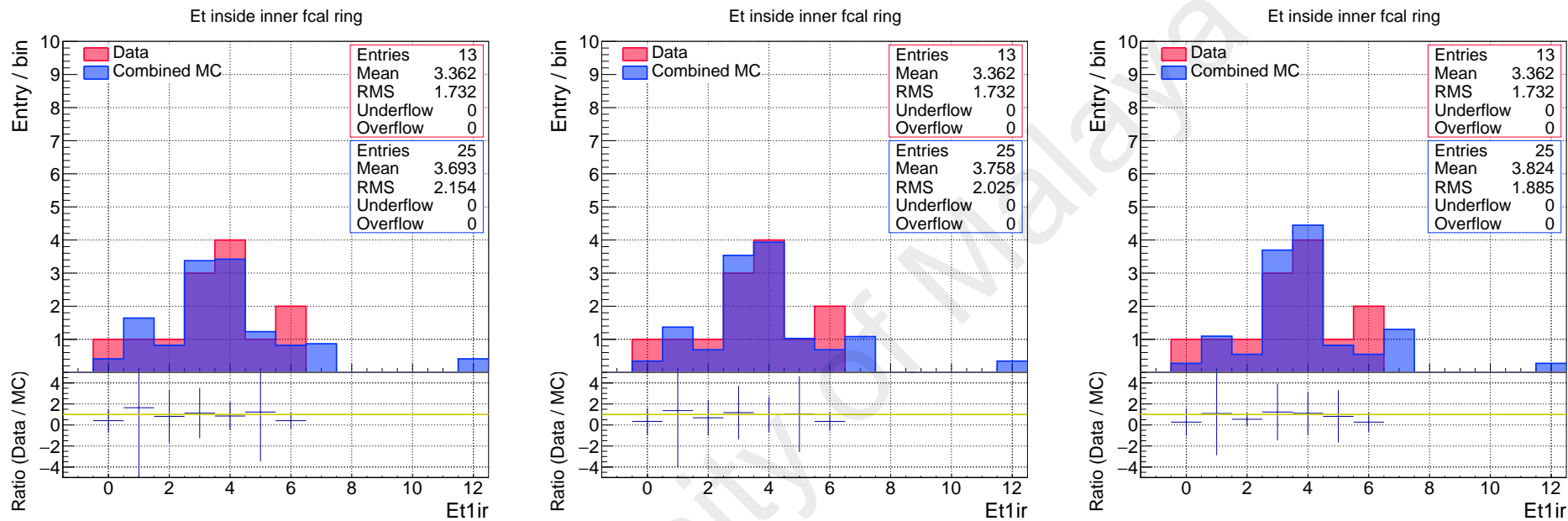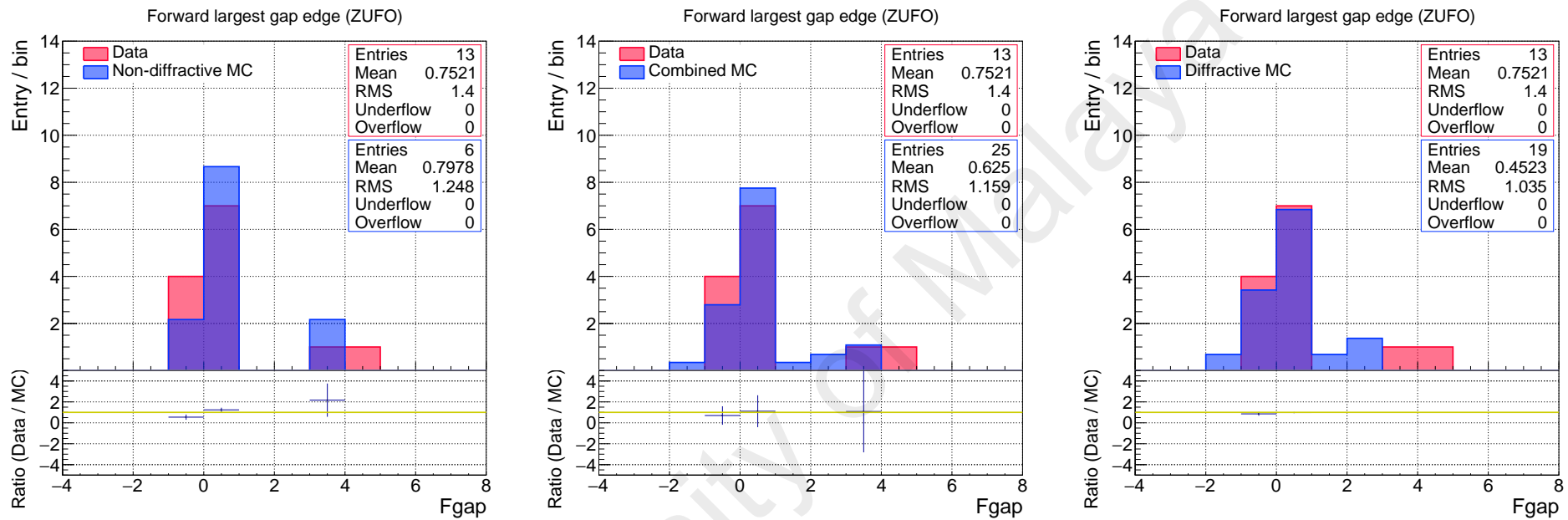
Figure 6.11: Comparison of data and combined MC of transverse energy variable for ratio 0.4:0.6 (left), 0.5:0.5 (middle), 0.6:0.4 (right).
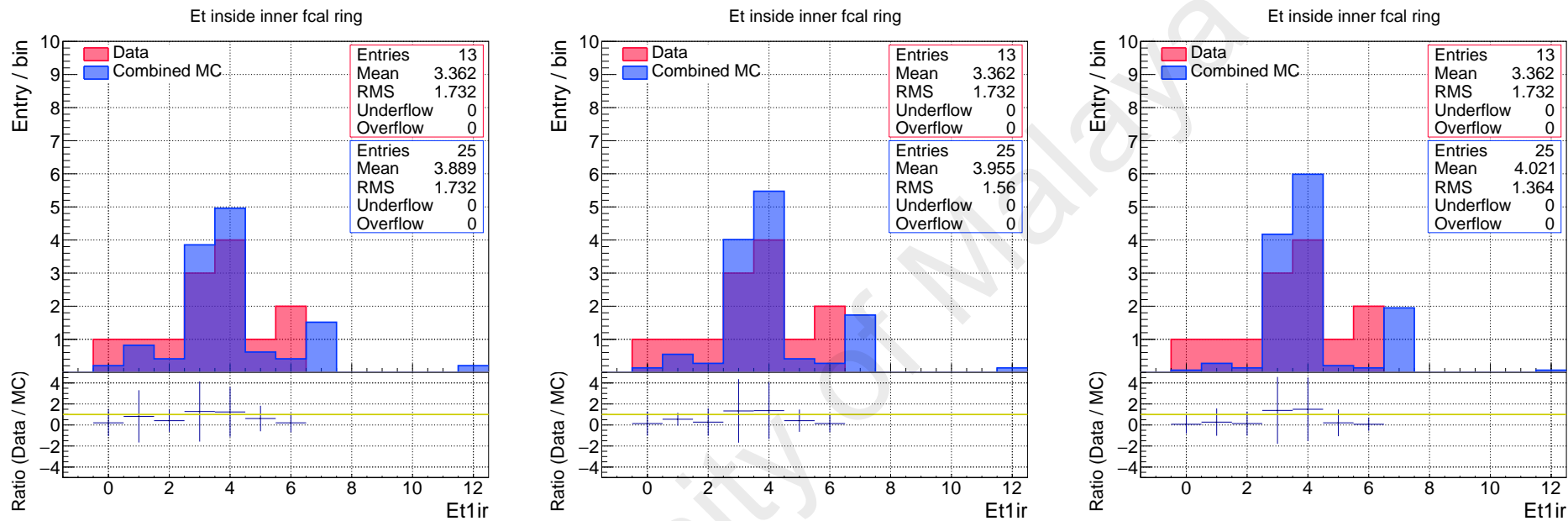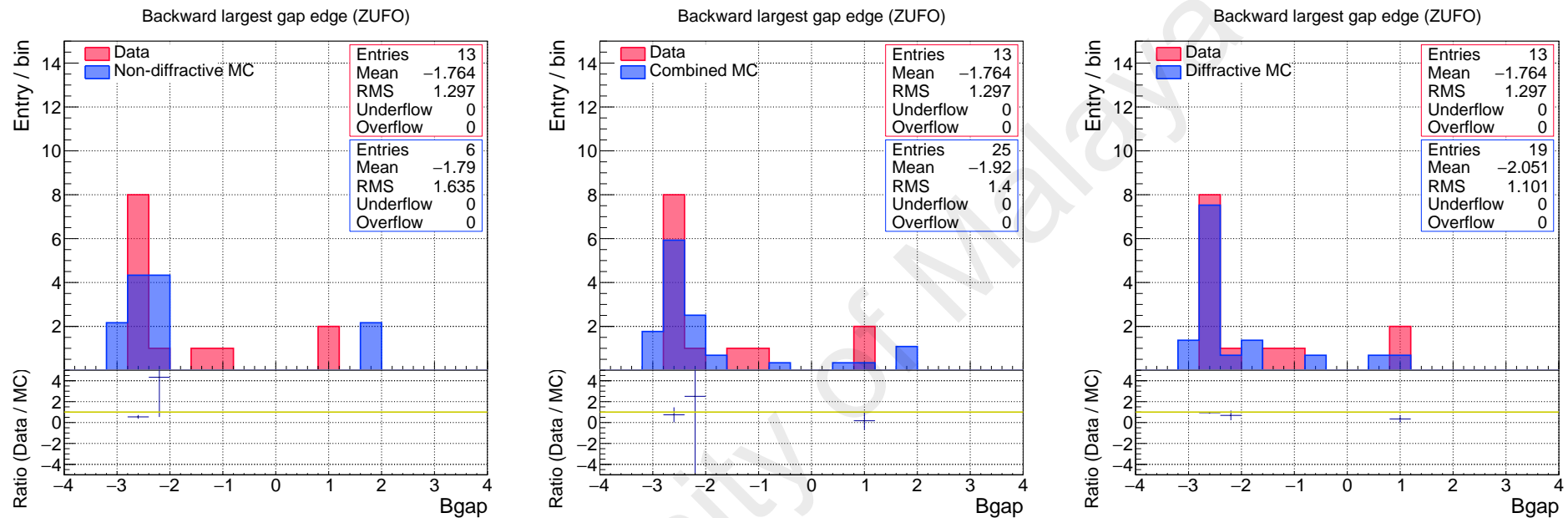
Figure 6.12: Comparison of data and combined MC of transverse energy variable for ratio 0.7:0.3 (left), 0.8:0.2 (middle), 0.9:0.1 (right).
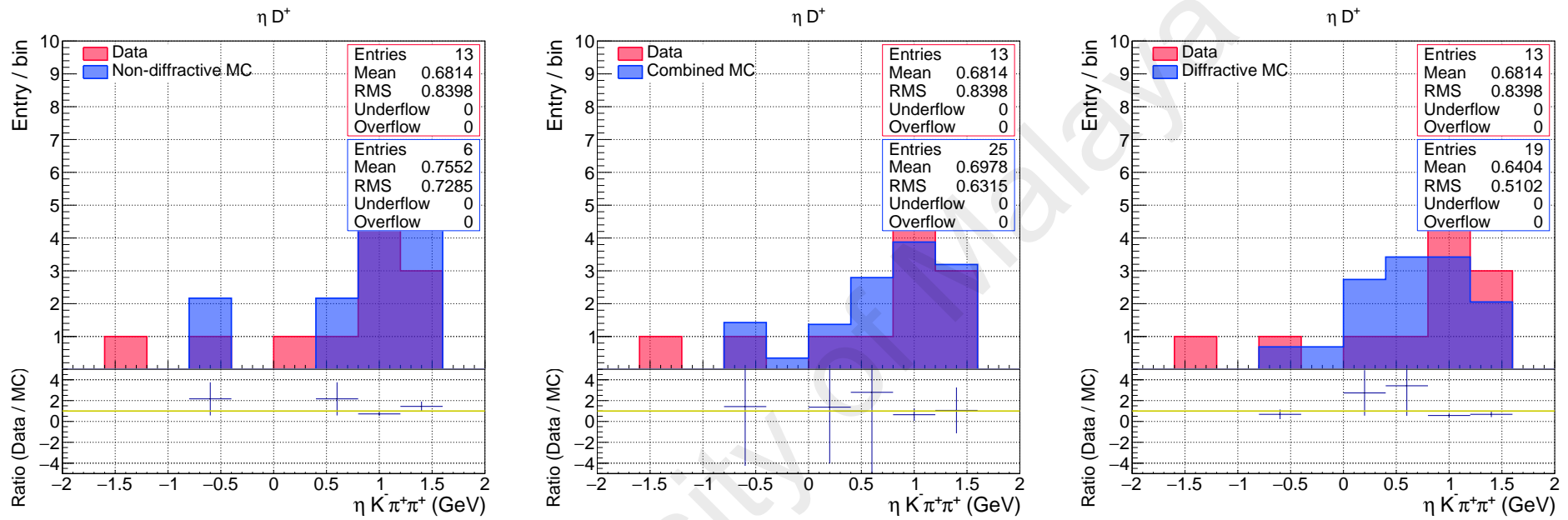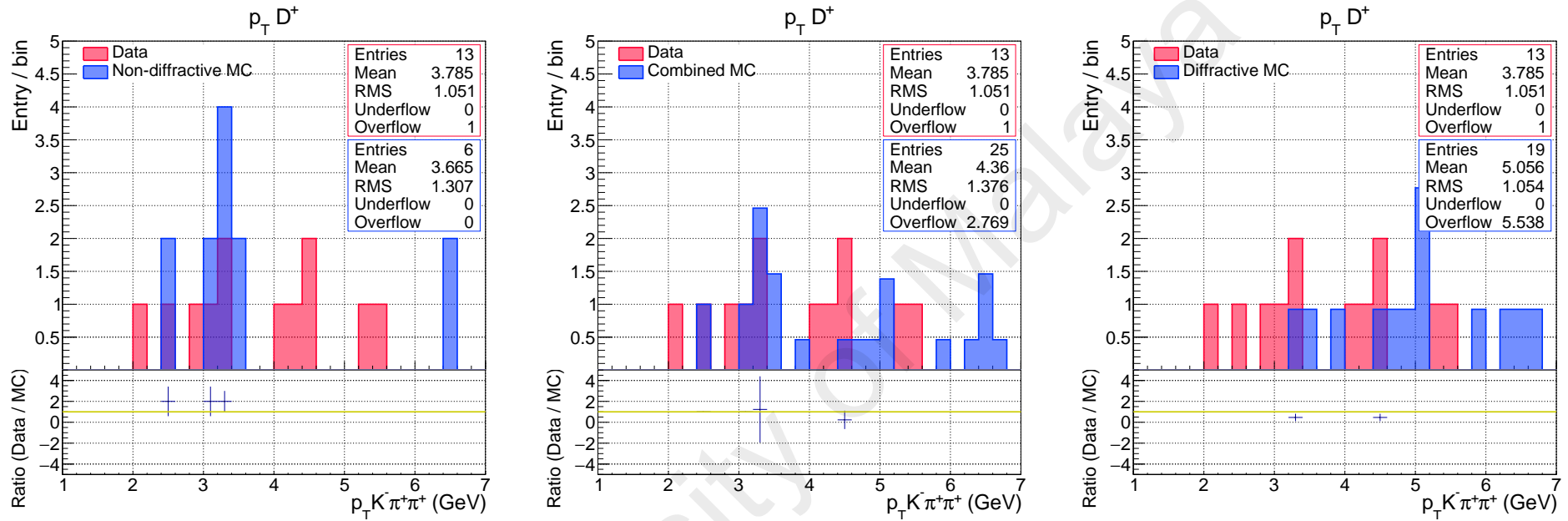
Figure 6.13: Comparison between data and each MC (left and right) as well as combination MC (middle) in forward largest gap.

Figure 6.14: Comparison between data and each MC (left and right) as well as combination MC (middle) in backward largest gap.
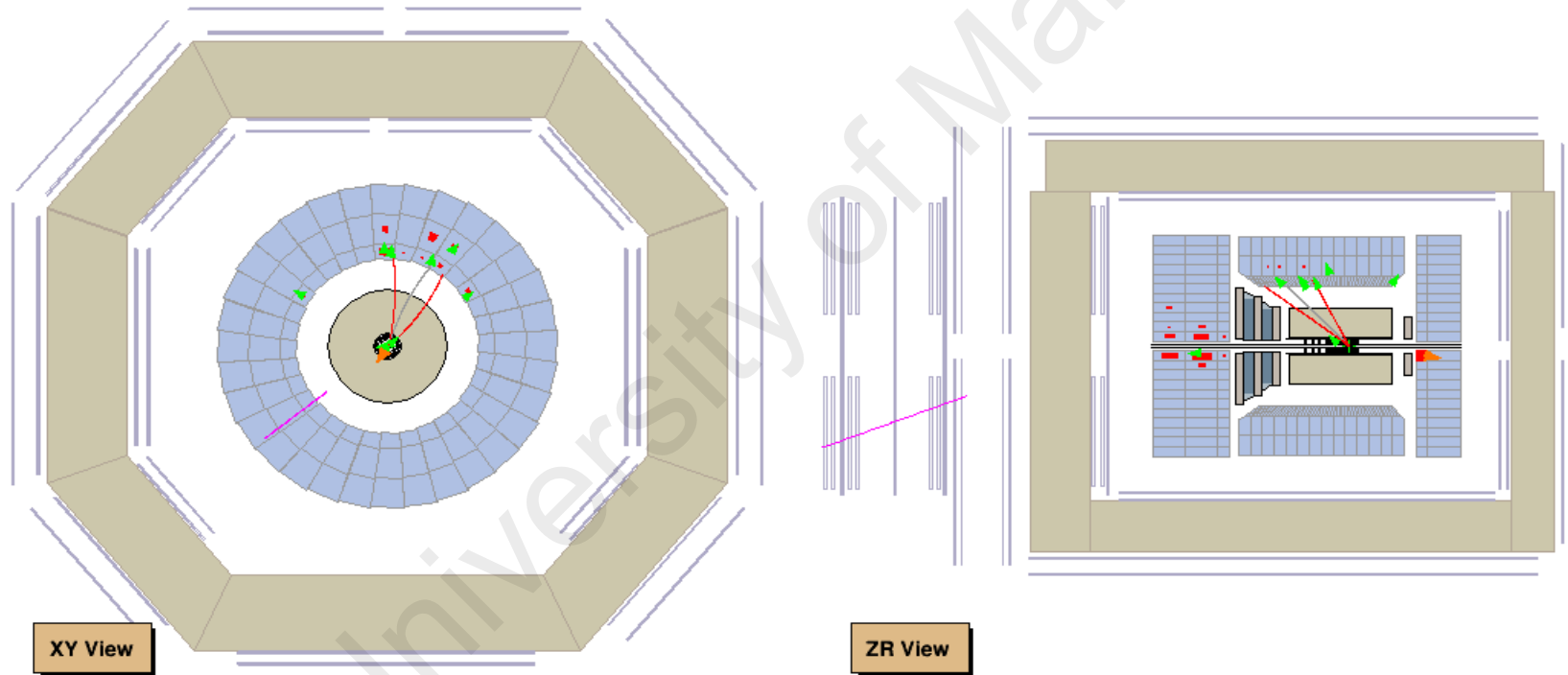
Figure 6.15: Comparison between data and each MC (left and right) as well as combination MC (middle) in pseudorapidity of D^+. It can be seen that most of the events are going forward and only a few events are going backward due to the asymmetry in the e-p collision.
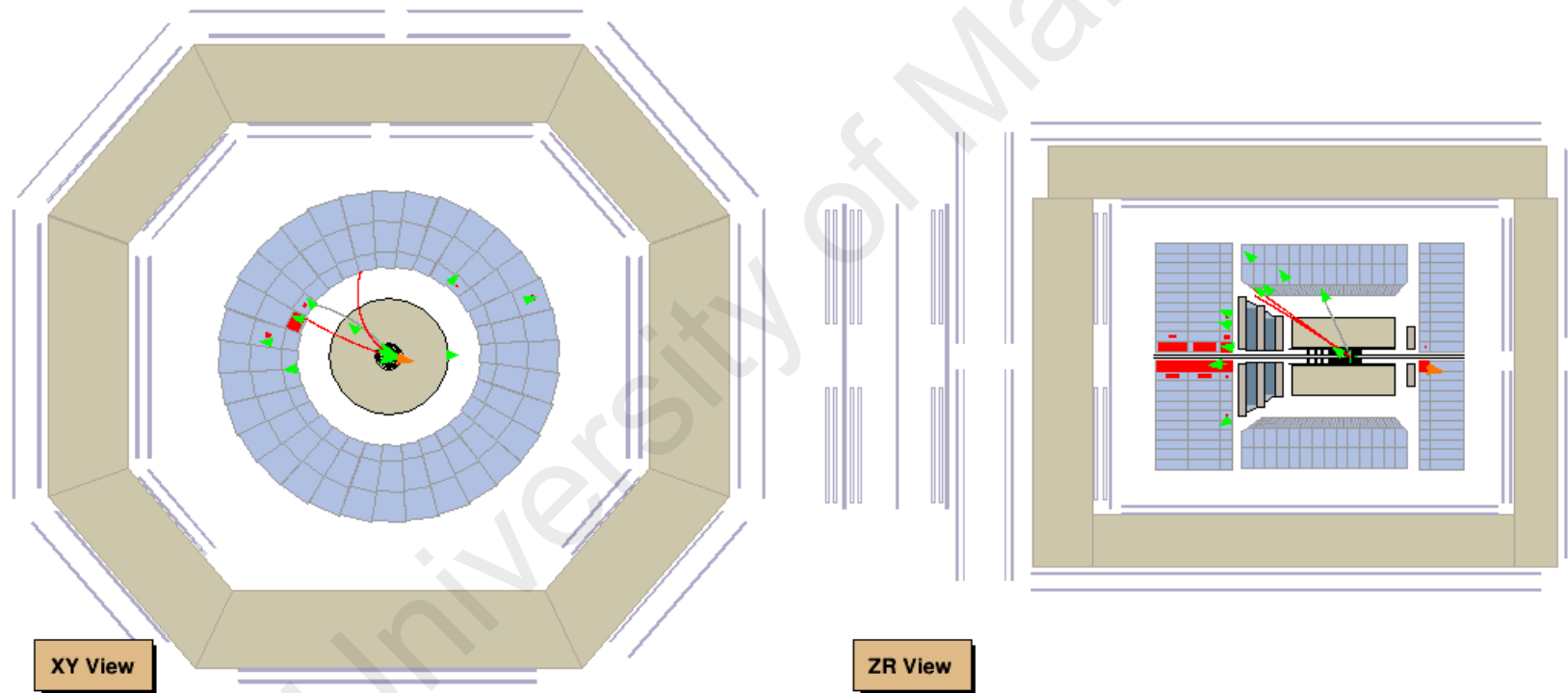
Figure 6.16: Comparison between data and each MC (left and right) as well as combination MC (middle) in $p_T D^+$. This analysis is conducted in the low p_T region. The distribution of $p_T D^+$ in diffractive MC started at $\pm$ 3 GeV because of the $p_T D^+$ preselection ($>$2.8 GeV) in the diffractive MC as mentioned previously.
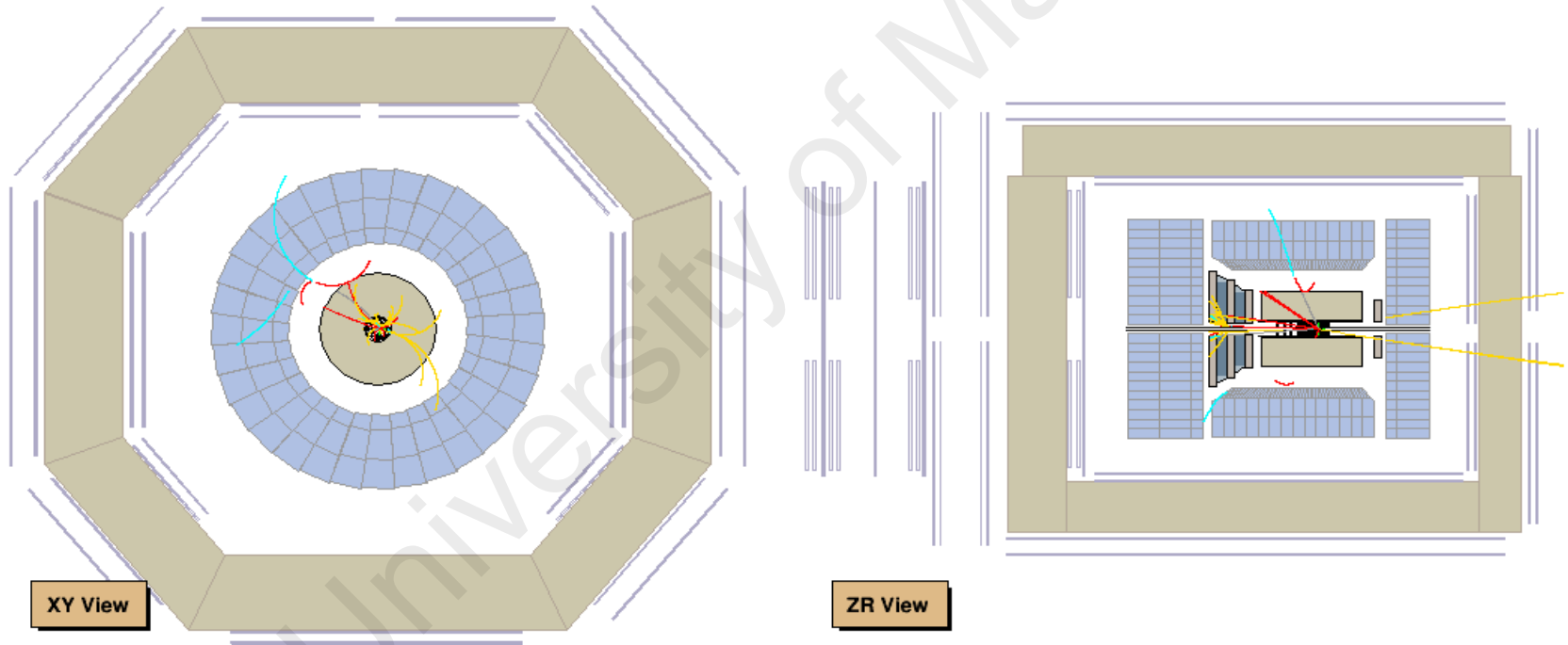
Figure 6.17: Data event with D⁻ meson is going forward with mass 1.86775 GeV. The figure is taken from this analysis in data using ZEUS Visualization (ZEVis) software.

Figure 6.18: Non-diffractive MC event with D^+ meson going forward with mass 1.8638 GeV. The figure is taken from this analysis in MC using ZEUS Visualization (ZEVis) software.

Figure 6.19: Non-diffractive MC true event with D meson going forward. The figure is taken from this analysis in MC using ZEUS Visualization (ZEVis) software.

$E=59$ GeV
$E_r=26.2$ GeV
phi=-2.11
$E_e^{SIRA}=26.2$ GeV
$y_{e,DA}^{SIRA}=0.06$

$E_t=10.8$ GeV
$p_t=0.862$ GeV
$t_f=2.9$ ns
$\theta_e^{SIRA}=2.96$
$Q_{e,SIRA}^{2,SIRA}=22.94$ GeV^2

$E-p_z=55.4$ GeV
$p_x=-0.443$ GeV
$t_b=0.0329$ ns
$\phi_e^{SIRA}=0.68$

$E_t=28.1$ GeV
$p_y=-0.74$ GeV
$t_r=0.422$ ns
$Prob_e^{SIRA}=0.999$

$E_b=4.74$ GeV
$p_z=3.68$ GeV
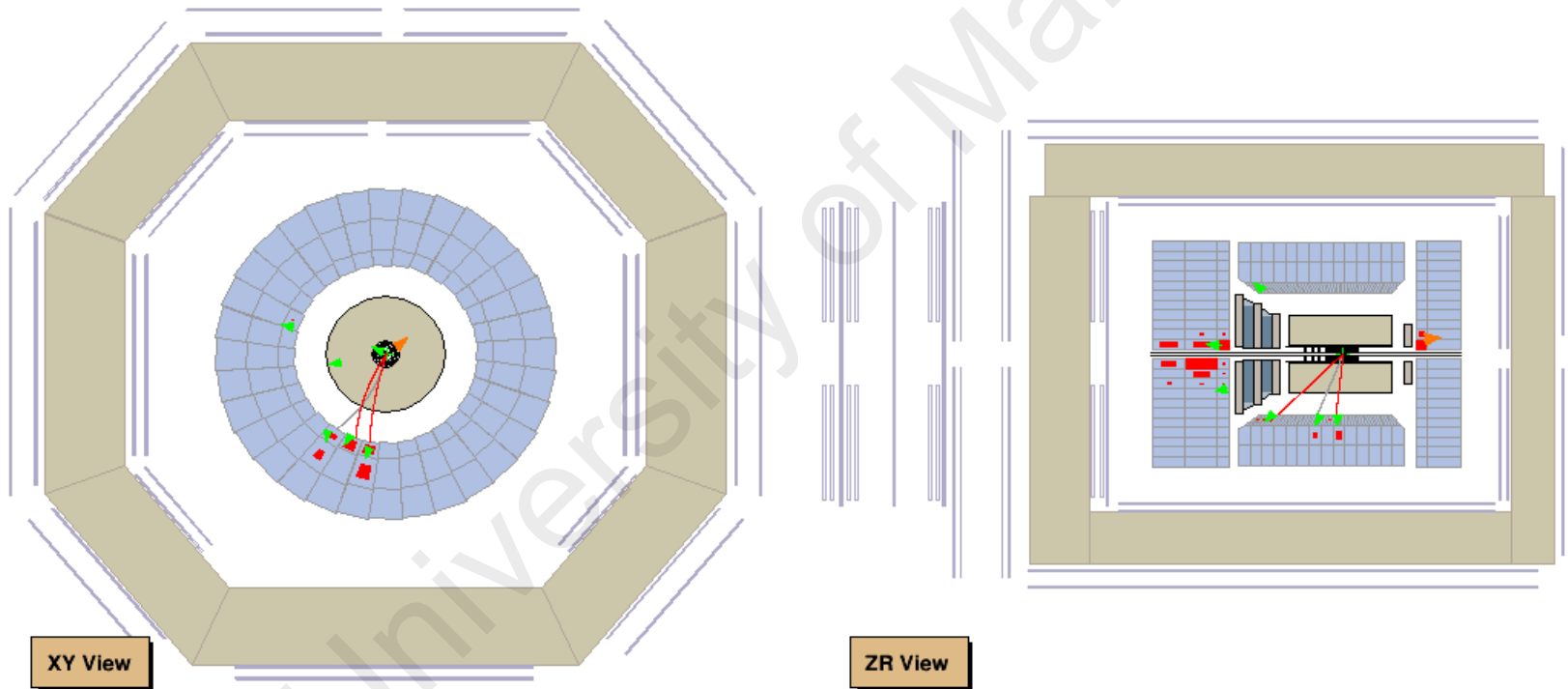$t_g=1.79$ ns
$x_{e,DA}^{SIRA}=0.00$

XY View

ZR View

Figure 6.20: Diffractive MC event with D^- meson going forward with mass 1.86915 GeV. The figure is taken from this analysis in MC using ZEUS Visualization (ZEVis) software.

Figure 6.21: Diffractive MC true event with D meson going forward. The figure is taken from this analysis in MC using ZEUS Visualization (ZEVis) software.
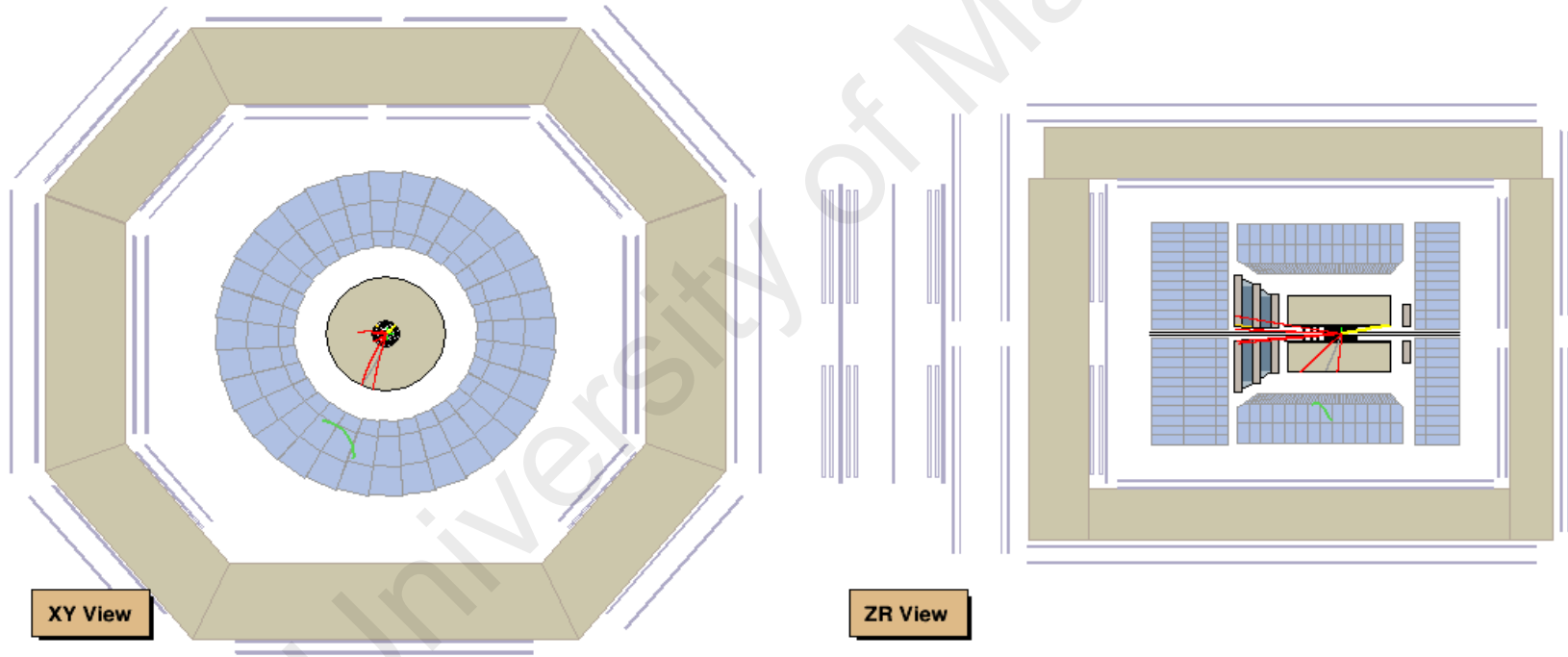
Figure 6.22: Data event with D^+ going backward with mass 1.87191 GeV. The figure is taken from this analysis in data using ZEUS Visualization (ZEVis) software.

Zeus Run 61234 Event 51516   date: 3-11-2006   time: 16:45:28

E=22 GeV
E_t=6.52 GeV
E-p_z=42.5 GeV
E_t=0 GeV
E_b=0.302 GeV

E_r=21.7 GeV
p_t=0.503 GeV
p_x=-0.47 GeV
p_y=0.18 GeV
p_z=-20.5 GeV

phi=2.78
t_f=-100 ns
t_b=-100 ns
t_r=0.0602 ns
t_g=0.0602 ns

E_g^{SIRA}=14.1 GeV
θ_e^{SIRA}=2.96
ϕ_e^{SIRA}=2.16
$Prob_e^{SIRA}$=0.999
$x_{e,DA}^{SIRA}$=0.00

$y_{e,DA}^{SIRA}$=0.36
$Q_{e,DA}^{2,SIRA}$=15.46 GeV^2

XY View

ZR View
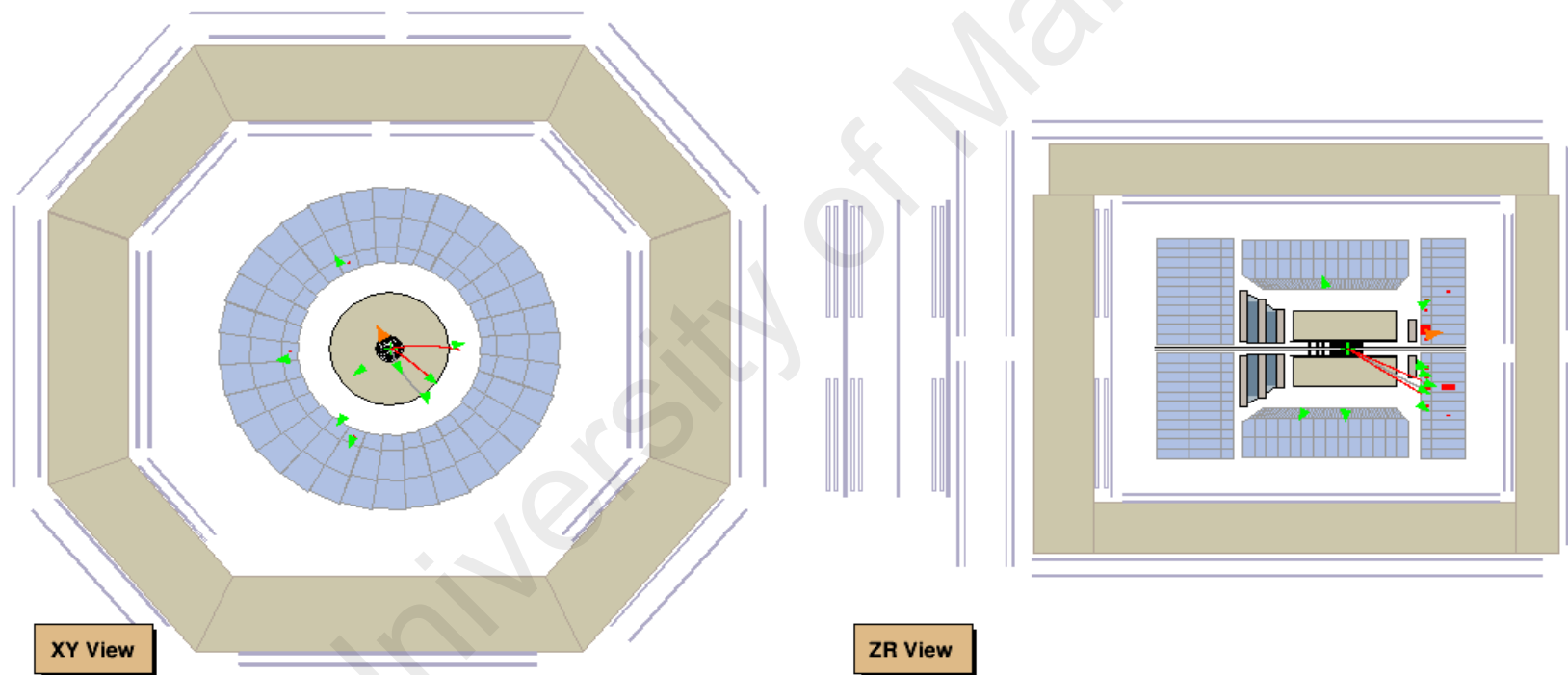
Figure 6.23: Data event with D^+ going backward with mass 1.87191 GeV. The figure is taken from this analysis in data using ZEUS Visualization (ZEVis) software.
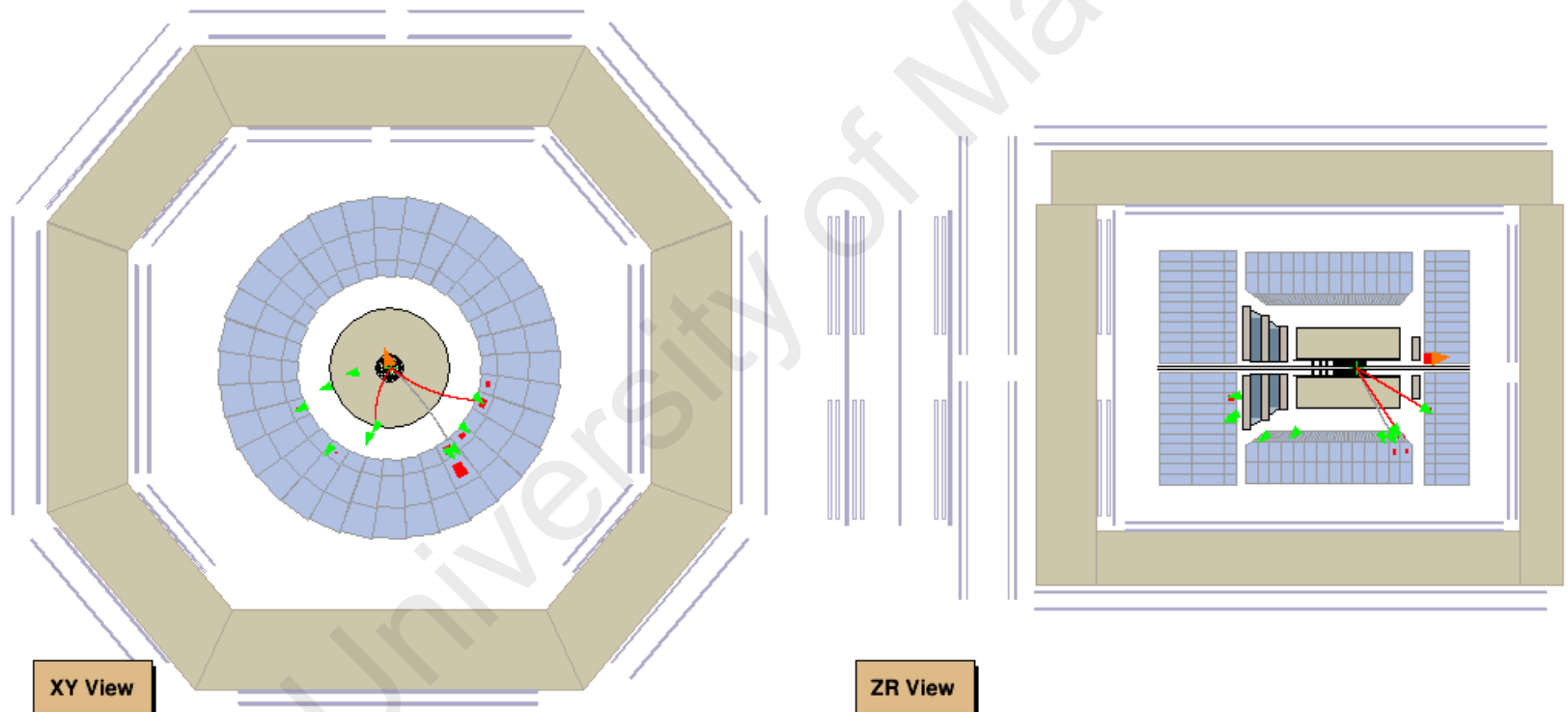
Figure 6.24: Diffractive MC event which particle going backward. The figure is taken from this analysis in MC using ZEUS Visualization (ZEVis) software.
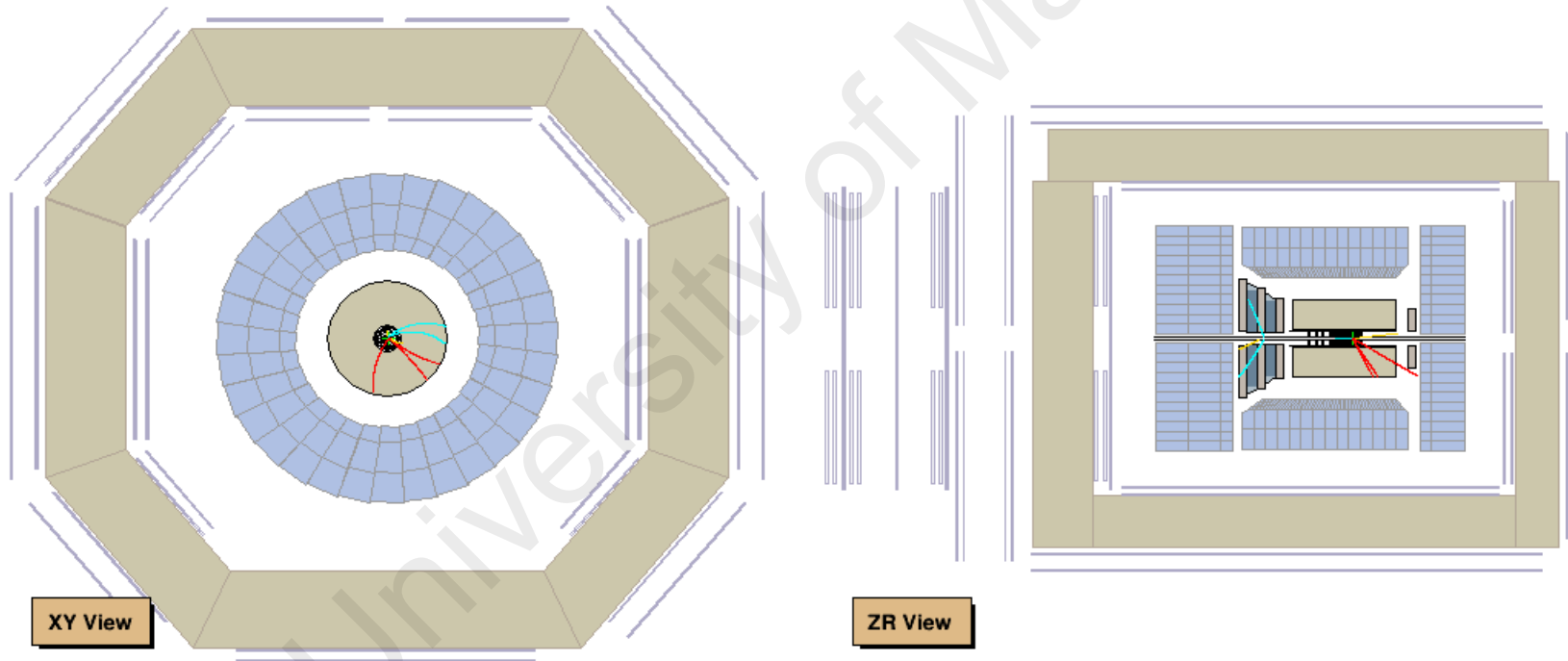
Figure 6.25: Diffractive MC true event particle with going backward. The figure is taken from this analysis in MC using ZEUS Visualization (ZEVis) software.

6.3.4 Forward activity in quasi-exclusive events

In the ZEVis, we have seen that only quasi-exclusive is observed with either the particles are going forward or backward in experimental data and MC. In Figure 6.14, there is some activity in the very forward region. As this activity is happening outside the tracker acceptance, one have to make use of MC truth information in order to determine the types of particles that are present in the calorimeter. From the previous result, it can be concluded that the MC description of the data is well-modelled. Table 6.1 and Table 6.2 show the list of particles from one of the events that passed the full event selection.

From the tables, one important observation is noted. The charm quark is actually produced in pairs. This applies also to the quasi-exclusive events under study in this project and the other charm hadron could not be reconstructed because it fell outside detector acceptance. Therefore, any hint of single charm production is not found, which is in line with SM expectations.

Table 6.1: List of particles from an event as displayed in Figure 6.19 and Figure 6.20.

Particle ID	Particle Type	Mother ID	p_T (GeV)	η	ϕ	Energy (GeV)
1	e^+	-	0.01554	-8.174	0.5121	27.56
2	p^+	-	0.5186	8.174	0.5121	920
3	Z^0	1	4.251	-0.2602	-0.3046	0.7775
4	e^+	1	4.262	-2.525	-0.302	26.78
5	d quark	2	0.05787	7.734	0.9209	66.1
6	gluon	5	0.3994	4.499	-0.2594	17.92
7	$\bar{c}$ quark	3	0.5506	3.826	1.38	12.72
8	c quark	3	3.952	0.926	-0.4481	5.963
9	$\bar{c}$ quark	7	0.5506	3.826	1.38	12.72
12	c quark	8	3.952	0.926	-0.4481	5.963
15	string	9	0.4913	5.482	1.452	59.15
16	$\bar{D}^0$	15	0.7442	4.058	0.5279	21.62
17	η meson	15	0.6021	3.603	-1.552	11.07
18	π^-	15	0.7539	4.251	0.706	26.46
19	string	12	4.698	5.903	-0.3269	861.6
20	D^+	19	3.281	1.022	-0.4951	5.479
21	π^-	19	0.0544	0.2697	0.4745	0.1505
22	π^+	19	0.5266	4.364	1.028	20.69
23	n	19	1.398	3.242	0.06229	17.94
24	$\bar{\Lambda}$	19	0.6537	4.457	-0.149	28.21
25	Σ_u^+	19	1.078	7.289	0.2845	789.1
26	K^+	16	0.6474	3.262	0.3265	8.476
27	π^-	16	0.1632	2.653	0.183	1.173
28	π^0	16	0.407	2.879	-0.2602	3.635

Table 6.2: List of particles from an event as displayed in Figure 6.15 and Figure 6.16 as continued from Table 6.1.

ParticleID	Particle Type	Mother ID	p_T (GeV)	η	ϕ	Energy (GeV)
29	π^0	16	0.3636	3.824	-0.9783	8.332
30	$\bar{K}^{*0}$	20	1.193	0.7603	-0.8433	1.779
31	π^+	20	2.198	1.11	-0.3088	3.7
32	γ	28	0.1857	2.617	-0.557	1.279
33	γ	28	0.2357	2.993	-0.02772	2.356
34	γ	29	0.2191	3.469	-0.9096	3.522
35	γ	29	0.1458	4.189	-1.082	4.81
36	K^-	30	0.7467	0.4252	-0.9752	0.953
37	π^+	30	0.4634	1.164	-0.6296	0.8264
38	p^+	25	1.094	7.072	0.3336	644.6
39	π^0	25	0.09248	8.048	-0.8874	144.6
40	γ	39	0.01359	5.508	-1.562	1.676
41	γ	39	0.1034	7.924	-0.9696	142.9
42	p^-	24	0.495	4.48	0.01052	21.85
43	π^+	24	0.1542	4.412	-0.5257	6.358
108	π^0	17	0.1633	3.128	1.13	1.871
109	π^0	17	0.2777	3.253	-1.411	3.598
110	π^0	17	0.1839	4.109	-1.371	5.604
111	γ	110	0.04411	2.946	-0.6012	0.4209
112	γ	110	0.1553	4.201	-1.57	5.184
136	γ	109	0.2674	3.286	-1.411	3.581
137	γ	109	0.01026	1.144	-1.386	0.01773
138	γ	108	0.06691	2.206	0.4209	0.3074
139	γ	108	0.1206	3.254	1.5	1.564

CHAPTER 7: CONCLUSION AND OUTLOOK

The D^+ production in DIS at the ZEUS experiment have been studied and the objectives have been achieved. Firstly, inclusive D^+ is reproduced and compared with the ZEUS published paper. This step is done to ensure the reconstruction of the D^+ is on the right track. The result shows that the reproduced D^+ mass distribution is compatible with the paper. The data and MC (non-diffractive) of inclusive D^+ are also compared with and without the reflection subtraction and significance cut. The cut that reduced most of the background is decay length significance cut where this cut was taken into account the D^+ projected decay length from the primary vertex to the secondary vertex and its uncertainty to ensure the accuracy of the selected D^+.

The next step is to search for exclusive D^+. From the definition of exclusive used in this analysis, only events that produced D^+ should be observed. To select these events, the so called exclusive cut is implemented, where since D^+ decays to $K^-\pi^+\pi^+$, only events with three tracks are selected. Another possible track is the four track where an additional track is the scattered electron track. This is because this analysis is the NC DIS process where electron should be included in the final state (see Figure 2.1).

Exclusive D^+ is unexpected to be seen, therefore only qualitative research is being done in this analysis. Several approaches are conducted to understand the exclusive D^+. First, an additional MC (diffractive) is used to compare with the data. Second, the comparison of data with non-diffractive MC, data with combined MC and data with diffractive MC in the mass range are shown where all of these plots. The events in data are reasonably described by the MC and the rough estimate for the fraction of events from non-diffractive and diffractive mixture is 0.5 ± 0.2.

To view the event in the detector, ZEVis software is used for both MC and experimental data. The result show that only quasi-exclusive D^+ is observed. This is because

of the other activities located at the very forward region. To understand what is this other activities, MC true events in ZEVis is shown and it is found that the main other particles come from the $\bar{D}^0$, $\bar{\Lambda}$ and Σ_u^+. The other important remark is the charm quark in D^+ is produced in pairs as SM predictions.

In the future, this study can be extend by focusing in truly exclusive region, where one can remove the activity in the forward region of the calorimeter. Since the main problem for this study is the lack of statistics, one can searching for the other D meson such as D^0 as it has higher cross section.

REFERENCES

Abramowicz, H., & Caldwell, A. (1999). HERA collider physics. *Reviews of Modern Physics*, *71*, 1275-1410.

Abramowicz, H., Caldwell, A., & Sinkus, R. (1995). Neural network based electron identification in the ZEUS calorimeter. *Nuclear Instruments and Methods in Physics Research Section A: Accelerators, Spectrometers, Detectors and Associated Equipment*, *A365*, 508-517.

Abramowicz, H., et al. (2015). Combination of measurements of inclusive deep inelastic $e^{\pm}p$ scattering cross sections and QCD analysis of HERA data. *European Physical Journal*, *C75*(12), 580.

Abt, I., et al. (1997). The H1 detector at HERA. *Nuclear Instruments and Methods in Physics Research Section A: Accelerators, Spectrometers, Detectors and Associated Equipment*, *A386*, 310-347.

Abt, I., et al. (2013). Measurement of $D^{\pm}$ production in deep inelastic *ep* scattering with the ZEUS detector at HERA. *Journal of High Energy Physics*, *05*, 023.

Ackerstaff, K., et al. (1998). The HERMES spectrometer. *Nuclear Instruments and Methods in Physics Research Section A: Accelerators, Spectrometers, Detectors and Associated Equipment*, *A417*, 230-265.

Adamczyk, L., et al. (2014). Measurement of the luminosity in the ZEUS experiment at HERA II. *Nuclear Instruments and Methods in Physics Research Section A: Accelerators, Spectrometers, Detectors and Associated Equipment*, *A744*, 80-90.

Aid, S., et al. (1995). Comparison of deep inelastic scattering with photoproduction interactions at HERA. *Physics Letter*, *B358*, 412-422.

Andresen, A., et al. (1991). Construction and beam test of the ZEUS forward and rear calorimeter. *Nuclear Instruments and Methods in Physics Research Section A: Accelerators, Spectrometers, Detectors and Associated Equipment*, *A309*, 101-142.

Bachynska, O. (2012). *Measurement of the $D^{*\pm}$ meson production in deep-inelastic scattering at HERA* (Doctoral dissertation, Hamburg U.) Retrieved from http://www-library.desy.de/cgi-bin/showprep.pl?thesis12-045.

Bailey, D. C., Bandyopadhyay, D., Benard, F., Bhadra, S., Chlebana, F., Crombie, M., . . . Teuscher, R. (1992). The ZEUS third level trigger hardware architecture. In *International Conference on Open Bus Systems 92 Zurich, Switzerland, October 13-15, 1992.* Retrieved from http://alice.cern.ch/format/showfull?sysnb=0160898.

Behnke, O., et al. (2015). Charm, beauty and top at HERA. *Progress in Particle and Nuclear Physics*, *84*, 1-72.

Bentvelsen, et al. (1992). Reconstruction of (x, Q^2) and extraction of structure functions in neutral current scattering at HERA. In *Workshop on Physics at HERA Hamburg, Germany, October 29-30, 1991* (p. 0023-42).

Beringer, J., et al. (2012). Review of particle physics (RPP). *Physical Review*, *D86*, 010001.

Bjorken, J. D. (1969). Asymptotic sum rules at infinite momentum. *Physical Review*, *179*, 1547-1553.

Bjorken, J. D., & Paschos, E. A. (1969, Sep). Inelastic electron-proton and γ-proton scattering and the structure of the nucleon. *Physical Review*, *185*, 1975–1982.

Brandelik, R., et al. (1979). Evidence for planar events in e+ e- annihilation at high-energies. *Physics Letter*, *B86*, 243.

Caldwell, A., et al. (1992). Design and implementation of a high precision readout system for the ZEUS calorimeter. *Nuclear Instruments and Methods in Physics Research Section A: Accelerators, Spectrometers, Detectors and Associated Equipment*, *A321*, 356-364.

Callan, C. G., & Gross, D. J. (1969, Jan). High-energy electroproduction and the constitution of the electric current. *Physical Review Letter*, *22*, 156–159. Retrieved from http://link.aps.org/doi/10.1103/PhysRevLett.22.156.

Chekanov, S., et al. (2009). Measurement of D+- and D0 production in deep inelastic scattering using a lifetime tag at HERA. *European Physical Journal*, *C63*, 171-188.

Derrick, M., et al. (1991). Design and construction of the ZEUS barrel calorimeter. *Nuclear Instruments and Methods in Physics Research Section A: Accelerators, Spectrometers, Detectors and Associated Equipment*, *A309*, 77-100.

Feynman, R. P. (1969). Very high-energy collisions of hadrons. *Physical Review Letter*, *23*, 1415-1417.

Foster, B., et al. (1993). The performance of the ZEUS central tracking detector z-by-timing electronics in a transputer based data acquisition system. *Nuclear Physics Proceeding Supply*, *32*, 181-188.

Foster, B., et al. (1994). The design and construction of the ZEUS central tracking detector. *Nuclear Instruments and Methods in Physics Research Section A: Accelerators, Spectrometers, Detectors and Associated Equipment*, *A338*, 254-283.

Fourletov, S. (2004). Straw tube tracking detector (stt) for zeus. *Nuclear Instruments and Methods in Physics Research Section A: Accelerators, Spectrometers, Detectors and Associated Equipment*, *535*(1–2), 191 - 196. Retrieved from http://www.sciencedirect.com/science/article/pii/S0168900204016006. (Proceedings of the 10th International Vienna Conference on Instrumentation)

Fruhwirth, R. (1987). Application of Kalman filtering to track and vertex fitting. *Nuclear Instruments and Methods in Physics Research Section A: Accelerators, Spectrometers, Detectors and Associated Equipment*, *A262*, 444-450.

Fruhwirth, R., & Strandlie, A. (1999). Track fitting with ambiguities and noise: A study of elastic tracking and nonlinear filters. *Computer Physics Communication*, *120*(2-3), 197-214.

Glashow, et al. (1970a). Weak interactions with lepton - hadron symmetry. *Physical Review*, *D2*, 1285-1292.

Glashow, et al. (1970b). Weak Interactions with Lepton-Hadron Symmetry. *Physical Review*, *D2*, 1285-1292.

Greenberg, O. W. (2008). The parton model. In *Compendium of Quantum Physics, ed. D. Greenberger, K. Hentschel and F. Weinert, (Springer-Verlag, Berlin Heidelberg, 2009),255-258.* Retrieved from http://inspirehep.net/record/785968/files/arXiv:0805.2588.pdf.

Grigorescu, T. G. (2008). *Measurement of charm production in deep inelastic scattering at HERA II* (Doctoral dissertation, Amsterdam U.) Retrieved from http://www-spires.fnal.gov/spires/find/books/www?cl=THESIS-GRIGORESCU.

Hartner, G. (talk at the ZEUS collaboration meetinga). *VCTRAK: STT(+CTD)+MVD combined pattern recognition.* (October 2005)

Hartner, G. (talk at the ZEUS collaboration meetingb). *VCTRAK: STT(+CTD)+MVD combined pattern recognition.* (February 2006)

Hartner, G. (ZEUS-98-058 (1998)). *VCTRAK Briefing: Program and Math (unpublished).* (Internal ZEUS note)

HERA-B, C. (1995). Hera-b: An experiment to study cp violation in the b system using an internal target at the hera proton ring. *Design report*.

HERA-B, C. (2000). Hera-b: Report on status and prospects october 2000. *Executive summary*.

Jacquet, F., & Blondel, A. (U. Amaldi (ed.), p. 391. Hamburg, Germany (1979). Also preprint DESY 79/48). Detection of the Charged Current Event - Method II. In *Proceedings of the Study for an ep Facility for Europe* (U. Amaldi ed.).

Jung, H. (1995). Hard diffractive scattering in high energy ep collisions and the monte carlo generator rapgap. *Computer Physics Communications*, *86*(1), 147 - 161.

Lisovyi, M. (2011). *Measurement of charm production in deep inelastic scattering using lifetime tagging for $D^{\pm}$ meson decays with the ZEUS detector at HERA* (Doctoral dissertation, Hamburg U.) Retrieved from http://www-library.desy.de/cgi-bin/showprep.pl?thesis11-033.

Maddox, E. (ZEUS-03-008 (2003)). *A Kalman filter track fit for the ZEUS microvertex detector (unpublished).* (Internal ZEUS note)

Metropolis, N., & Ulam, S. (1949). The monte carlo method. *Journal of the American Statistical Association*, *44*(247), 335-341.

Polini, A., et al. (2007). The design and performance of the ZEUS Micro Vertex detector. *Nuclear Instruments and Methods in Physics Research Section A: Accelerators, Spectrometers, Detectors and Associated Equipment*, *A581*, 656-686.

Roloff, P. (2011). *Measurement of charm and beauty production in deep inelastic scattering at HERA* (Doctoral dissertation, Hamburg U.) Retrieved from http://www-

library.desy.de/cgi-bin/showprep.pl?thesis11-049.

Smith, W. H., et al. (1995). The ZEUS calorimeter first level trigger. *Nuclear Instruments and Methods in Physics Research Section A: Accelerators, Spectrometers, Detectors and Associated Equipment*, *A355*, 278-294.

Smith, W. H., Tokushuku, K., & Wiggers, L. W. (1992). The ZEUS trigger system. In *6th International Conference on Computing in High-Energy and Nuclear Physics (CHEP 1992) Annecy, France, Sept 21-25, 1992.*

Spiridonov, A. (2008). Mathematical framework for fast and rigorous track fit for the ZEUS detector.

Tuning, N. (ZEUS-01-021 (2001)). *ZUFOs: Hadronic Final State Reconstruction with Calorimeter, Tracking and Backsplash Correction (unpublished).* (Internal ZEUS note)

Uijterwaal, H. A. J. R. (1992). *The global second level trigger for ZEUS* (Unpublished doctoral dissertation). Amsterdam U.

Verena, S. (2006). Available on http://www-zeus.desy.de/ vschoenb/.

Weinberg, S. (1967). A model of leptons. *Physical Review Letter*, *19*, 1264-1266.

Weinzierl, S. (2000). Introduction to Monte Carlo methods. Retrieved from https://arxiv.org/abs/0905.1629.

Whyte, J. I. (2008). *Charm production and F2(c anti-c) measurements in deep inelastic scattering at HERA II* (Unpublished doctoral dissertation). York U., Canada.

Wilton, R. H., et al. (1999, May). *The ctd tracking resolution* (Internal note No. 99-024). Hamburg: ZEUS.

ZEUS, C. (1993). *The zeus detector: Status report.* Retrieved from http://www-zeus.desy.de/bluebook/bluebook.html.